

---

# Preparations for study of ordering in aqueous suspensions of a nano-layered synthetic silicate

*Nils Ivar Ringdal*

Supervisor: Professor Dr.ing Jon Otto Fossum

---



## **Abstract**

This project is build on previously work done on phase shifts and observations of orientational ordering in aqueous suspensions of nano-layered silicate clays. For those work scattering experiments and some visual observations have been carried out of Na-fluorohectorite dispersed in salt-solution when the system has phase separated. The focus for this project has been to visually time record the phase shift process and further dynamics as it is settling under gravity. With the use of todays single lens reflex digital camera technology, the process for such a visual recording is a lot simpler than it would had been some years ago with the same quality to the results. A total of 11 700 pictures have been taken distributed on 40 different samples. The sample solutions are made by vary the clay weight percentage across different NaCl concentrations. The use of two different Na-fluorohectorite powders with different crushing properties have given large distinctions for samples having the exact clay amount and salt solution. The use of a 1 Tesla gap magnet for two sample settling, gave some increase in birefringence to the sample being most crushed. For all samples, pictures have been taken continuously from the sample creation. Most samples have been photographed two times per day, while some selected samples has been recorded with a new picture like every 20 minutes. With this material, movies for almost every sample has been made. With the movies, the dynamics of nematic phases can be studied. For two samples of each powder type, the different phases has been weighted up as function of sample height.

## Preface

This written report, together with the enclosed DVDs, makes up the documentation for the compulsory project work in the ninth semester for the study of Master in Technology ("Sivilingeniør") at the Norwegian University of Technology and Science (NTNU).

I would like to acknowledge very much my supervisor, Professor Jon Otto Fossum for introduction and guidance of the project. I will also thank Post. Doc Ahmed Gmira for start up in the summer and later discussion of the project. At last, I thank Arnolf Bjølstad and the people at the Instrumental Workshop for doing a great job creating my experimental equipment.

Trondheim, desember 2006

*Nils Ivar Ringdal*

# Contents

<b>1 Theory</b>	<b>1</b>
1.1 Clay . . . . .	1
1.2 Na-fluorohectorite . . . . .	2
1.3 Cation exchange . . . . .	2
1.4 Clay salt suspensions to optical observations . . . . .	3
1.5 local orientational correlations . . . . .	4
1.6 DLVO-theory . . . . .	5
1.6.1 Attractive Van der Waals and repulsive double layer forces . . . . .	5
1.6.2 The role of salt concentration and aggregation . . . . .	7
1.7 Gels . . . . .	10
1.8 Liquid Crystals . . . . .	11
1.8.1 Characterizing Liquid Crystals . . . . .	12
1.8.2 Liquid Crystal Phases . . . . .	13
1.8.3 Electric and Magnetic Field Effects . . . . .	15
1.8.4 Chemical Properties of Liquid Crystals . . . . .	16
1.8.5 Light and Polarization . . . . .	16
1.8.6 Isotropic-nematic transition . . . . .	21
1.8.7 Applications of liquid crystals . . . . .	22
<b>2 Experiment</b>	<b>24</b>
2.1 Na-Fluorohectorite powder preparations . . . . .	24
2.2 Vitrotube . . . . .	24
2.3 Polarizers . . . . .	25
2.4 Canon EOS 350D . . . . .	26
2.5 Experimental Setup . . . . .	27
2.5.1 Cardboard setup . . . . .	27
2.5.2 Metal stage setup . . . . .	28
2.6 UVP white light transilluminator . . . . .	29
2.7 Magnet . . . . .	29
2.8 Weighing of different phases . . . . .	30
2.9 Computer softwares . . . . .	30
<b>3 Results and Discussion</b>	<b>31</b>
3.1 Sample distribution . . . . .	31
3.2 Comparison across concentrations . . . . .	32
3.3 Comparison of w/w% . . . . .	37
3.4 Time progress . . . . .	43
3.5 Magnetic study . . . . .	46
3.6 Mass distribution of sample . . . . .	46

<b>A Electromagnetic waves in an anisotropic material</b>	<b>52</b>
<b>B Drawings</b>	<b>54</b>
B.1 Rack . . . . .	56

# Chapter 1

## Theory

### 1.1 Clay

Clay is a term used to describe a group of hydrous aluminum phyllosilicate<sup>1</sup> minerals, that are typically less than 2  $\mu\text{m}$  in diameter. Clay consists of a variety of phyllosilicate minerals rich in silicon and aluminium oxides and hydroxides which include variable amounts of structural water. Clays are generally formed by the chemical weathering of silicate-bearing rocks by carbonic acid but some are formed by hydrothermal activity. Clays are distinguished from other small particles present in soils such as silt by their small size, flake or layered shape, affinity for water and tendency toward high plasticity. Depending upon academic source, there are three or four main groups of clays: kaolinite<sup>2</sup>, montmorillonite-smectite<sup>3</sup>, illite<sup>4</sup>, and chlorite<sup>5</sup>. There are about thirty different types of 'pure' clays in these categories but most natural clays are mixtures of these different types, along with other weathered minerals.

Like all phyllosilicates, clay minerals are characterised by two-dimensional sheets of corner sharing  $\text{SiO}_4$  and  $\text{AlO}_4$  tetrahedra. Each tetrahedron shares 3 of its vertex oxygen atoms with other tetrahedral. The fourth vertex is not shared with another tetrahedron and all of the tetrahedra "point" in the same direction (i.e. all of the unshared vertices are on the same side of the sheet). These tetrahedral sheets have the chemical composition  $(\text{Al}, \text{Si})_3\text{O}_4$ .

In clays the tetrahedral sheets are always bonded to octahedral sheets formed from small cations, such as aluminium or magnesium, coordinated by six oxygen atoms. The unshared vertex from the tetrahedral sheet also form part of one side of the octahedral sheet but an additional oxygen atom is located above the gap in the tetrahedral sheet at the center of the six tetrahedra. This oxygen atom is bonded to a hydrogen atom forming an OH group in the clay structure. Clays can be categorised depending on the way that tetrahedral and octahedral sheets are packaged into layers. If there is only one tetrahedral and one octahedral group in each layer the clay is known as a 1:1 clay. The alternative, known as a 2:1 clay, has two tetrahedral sheets with the unshared vertex of each sheet pointing towards each other and forming each side of the octahedral sheet.

In 1972 the AIPEA Nomenclature committee agreed upon usage of the terms "plane,"

---

<sup>1</sup> phyllosilicates being a subgroup of silicate minerals

<sup>2</sup> Kaolinite group includes the minerals kaolinite, dickite, halloysite and nacrite.

<sup>3</sup> Smectite group includes pyrophyllite, talc, vermiculite, sauconite, saponite, nontronite and montmorillonite.

<sup>4</sup> Illite group includes the clay-micas. Illite is the only common mineral.

<sup>5</sup> the chlorite group is not always considered a part of the clays and is sometimes classified as a separate group within the phyllosilicates.

"sheet," "layer," "unit structure," and their equivalents in other languages [1]. Recommended usage is as a single plane of atoms, a tetrahedral or octahedral sheet, and a 1:1 or 2:1 layer. Thus, plane, sheet, and layer refer to increasingly thicker arrangements. A sheet is a combination of planes and a layer is a combination of sheets. In addition, layers may be separated from one another by various interlayer materials, including cations, hydrated cations, organic molecules, and hydroxide octahedral groups and sheets. The total assembly of a layer plus interlayer material is referred to as a unit structure.

Depending on the composition of the tetrahedral and octahedral sheets, the layer will have no charge, or will have a net negative charge. If the layers are charged this charge is balanced by interlayer cations such as Na<sup>+</sup> or K<sup>+</sup>. In each case the interlayer can also contain water. The crystal structure is formed from a stack of layers interspersed with the interlayers.

Clays sintered in fire were the first ceramic, and remain one of the cheapest to produce and most widely used materials even in the present day. Bricks, cooking pots, art objects, dishware and even musical instruments such as the ocarina are all made with clay. Common present day uses of 2:1 clays include building materials, ceramics, cement production, rheology modification, catalysis, paper making, oil well-drilling and other industrial processes.

## 1.2 Na-fluorohectorite

Na fluorohectorite is a synthetic 2:1 smectite clay having the nominal chemical formula Na<sub>0.6</sub>Mg<sub>2.4</sub>Li<sub>0.6</sub>Si<sub>4</sub>O<sub>10</sub>F<sub>2</sub>. Like natural hectorite<sup>6</sup> Na-Fh is a swelling clay that incorporate a variable amount of water in the interlayer space, resulting in a change in lattice constant along the stacking direction. Na-Fh has a rather large surface charge of 1.2 e<sup>-1</sup>/unit cell, compared to for example laponite (0.4 e<sup>-1</sup>/unit cell). The particle size of Na-Fh is quit large and can variable up to 20 000 Å in diameter. [2] Compared to natural clays such as montmorillonite, Na-Fh might be expected to have a more homogeneous composition and charge distribution. The polydispersity in particle size makes the Na-Fh suspensions particularly interesting, because gravitational forces effectively sort the particles by size, stabilizing in some cases several strata of gels, sols and/or sediments within a single sample tube.

## 1.3 Cation exchange

cation exchange capacity measures two of the fundamental properties of clays, the surface area and the charge on this area. The exchange capacity is an estimate of both the number of ions absorbed between the layers of a clay structure and of those adsorbed on the outer surfaces.

Addition of a small concentration of salt to a clay suspension (where particles remain in the aqueous medium through brownian motion) will tend to form particle aggregates. The process is called flocculation. The aggregates tend to become large and dense enough to settle and the clay water suspension is destroyed. This process is independent of the cation exchange by absorption (between the sheets of the clay particles).

The charge measured as being exchanged on sites between the layers of clays or within the structure varies between 40 and 120 meq. This value should be proportional to the charge on the layers induced by substitutions of ions which create an electrostatic charge imbalance on the silicate. One can distinguish two kinds of clay, those with low exchange

---

<sup>6</sup>A clay mineral similar in structure to bentonite but with more negative charges on its surface.

capacities(10 meq) and those with high capacities (40-120 meq). The quantity of ions present is recorded as the charge, milliequivalents, which are found to be fixed on 100 g of dried clay. The cation exchange capacity is given in milliequivalents per 100 g of dried material (meq/100 g or simply meq).

From cation exchange selectivity the interlayer ions are loosely held, so much that they can be interchanged in aqueous solution which contains a high proportion of another ion. The exact ration of ionic species in the solution will determine those in between the layers of the swelling clay. The proportion of one to another in each phase (aqueous and clay) determines the cation exchange isotherms of selectivity coefficients. The proportion of each site reflects the chemical activity of the ion in each substance. By thermodynamic definition, when the solution and the clay come into chemical equilibrium, the activity of the ions in each phase is the same. However, some ions prefer the clay to the solution when in the presence of other ions. For example, calcium much prefers clay over sodium or potassium. In general, the divalent ions are preferred in swelling clay interlayer sites to monovalent ones. The reverse is true for micas (with higes charges). If one changes the composition of the solution, for example, the clay interlayer ion composition will also change. For example, if the initial solution is at  $x$ , with 50% cation A, the clay composition will be 20%. If one change the solution composition to  $y$ , 75% A then the clay will contain 50% A. Both will increase their A cintent but not in the same proportions. The concept of ion exchage and cation partitioning is very important to studies which try to predict the chemical affinities and pathways during aqueous migrations.

## 1.4 Clay salt suspensions to optical observations

Smectite 2:1 clay particles dispersed in salt solutions have been studied for decades. In newer time the complex physical phenomena in clays have been of growing interest. The individual 2:1 particles are composed of one or more silicate lamellae (a layered plate-like structure) that stack by sharing exchangeable cations between their faces figure 1 (a) and (b). [4]

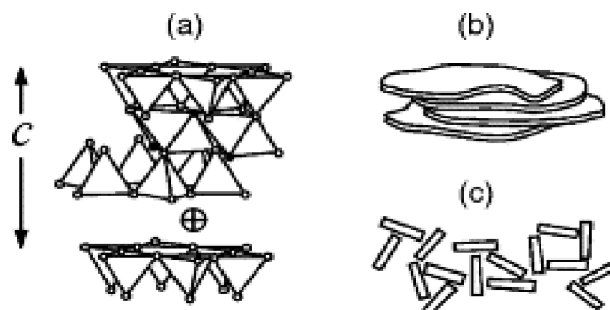


Figure 1.1: (a) A general sketch of the structure of the synthetic 2:1 swelling clay fluorohectorite. The structure are composed of oxygen (o), fluorine (●) and exchangeable cation (+) sites (b) Clay particle formed from stacked lamellae in the micron scale. (c) Face-to-edge and edge-to-edge aggregation of clay particles.[5]

Much effort has gone into relation the structural and rheological properties of clay-salt suspensions to optical observations, which find birefringent domains with defect textures characteristic of nematic liquid crystals. From a more fundamental point of view, the aqueous suspensions of disklike clay particles have been widely studied as model colloids[6, 7, 8, 9, 10, 11] and because they have a gel phase, the origin of which is still under

debate.[12, 13, 15] As early as 1938, Langmuir<sup>7</sup>[16] observed the occurrence of tactoids<sup>8</sup>, and eventually the coacervation of bentonite sols in two phases, one of which was a birefringent gel. He discussed these phenomena in relation with the liquid-crystalline phases newly discovered at that time, but he concluded that the birefringent phase had a three-dimensional cubic lattice rather than a nematic liquid-crystalline organization. In 1956, using optical microscopy, Emerson [17] observed in swollen clay flakes a banded texture somewhat similar to that displayed by the tobacco mosaic virus.

The swelling patterns in water and dilute salt sols, a new organo-clay complexes were observed. These complexes involve only the edge faces of clay crystals; this is termed peripheral complexing. Such complexes, as between bentonite and maleic acid-vinyl acetate copolymer, form highly vertically expanded gels similar to those with illite and kaolinite. Bentonite with added polyvinyl alc., which forms interlamellar complexes, gave less swelling than did the peripheral complexes. It is suggested that the polymer links the edge faces of the clay crystals in a series of H bonds to form the peripheral complexes. On the theoretical side, an Onsager transition to a nematic phase was indeed predicted in swollen clay suspensions. Subsequently, various scientists investigated aqueous clay suspensions by scattering[18]-[29] or NMR[30, 31, 32] experimental techniques, but they did not try to assess their possible liquid crystallinity. In 1996 Gabriel, Sanchez and Davidson [33] managed with simple optical observations to provide clear-cut evidence of the nematic liquid-crystal textures for natural bentonite and synthetic laponite B suspensions in the gel or solid phase. At low particle concentration, in the sol or liquid phase, the suspensions observed between cross-polarizers appeared isotropic. In the gel phase two successive domains are observed: an optically isotropic gel at low particle concentration and a permanent nematic one at a higher concentration. This study focused on the nematic liquid-crystal texture of laponite, but it did not shed light on the structure of the nonbirefringent gel phase and on the nature of the sol-gel transition.

Right after, Mourchid and Levitz [14] questioned the origin of the long-term gelation of laponite aqueous dispersions.

The sol-gel transition of laponite suspensions was also investigated using Monte Carlo simulations. Each charged particle of laponite and its double layer was considered to be a rigid point quadrupole. The numerical calculations showed a sol-gel transition when the particle concentration was increased. The structure of the model gel suspension was found to be compatible with the house of cards structure, proposed some years ago by Van Olphen, in which the particles are edge to face with each other and without any direct contact. However, no experimental evidence exists of such structure in the case of laponite suspensions and the computed phase diagram does not reproduce the salt effect.

## 1.5 local orientational correlations

By small angle neutron scattering Ramsay and Lindner [36](1993) investigated the structure and interparticle interactions in colloidal dispersions of montmorillonite and Laponite RD (a model hectorite-type clay). These measurements suggested the presence of local orientational correlations in these smectite clay gels. Direct *in situ* structural evidence for parallel alignment of platelets was present around the millennium shift. Gravity dispersed solutions from Na fluorohectorite was studied by synchrotron x-ray diffraction over a large NaCl concentration [34]. The use of liquid scattering technique made it possible identify

---

<sup>7</sup>Irving Langmuir was born in Brooklyn, New York in 1881. He won the Nobel Prize in Chemistry in 1932

<sup>8</sup>i.e., small birefringent domains floating in isotropic suspensions

regions in which particles reorient from horizontal to vertical alignments in strata coexisting at different heights within the sample. The experimentalist identified two distinct gel regions characterized by differences in orientaional anisotropy ans domain size. The results provided direct proof for nematic order, as well as unique structural information regarding particle morphology and alignment within each of the colloid phases. In another experiment by Lemaire et.al. the nematic order parameter on oriented samples of laponite clay gels (obtained by slow evaporation) was measured by small angle X-ray scattering experiments [35]. The SAXS patterns obtained was clearly anisotropic, which demonstrates the existence of nematic-like orientational correlations of the laponite disc-like particles. The value of the nematic order parameter, derived from the SAXS patterns is comparable to that of usual liquid crystals. This large value proves the importance of orientational correlations in these gels at concentrations higher than, even in the absence of shear.

Although the layered subunit is crystalline, relative registry and orientations between lamellae are usually quite disordered. Substitution of metals within the silicate layer produces a surface charge, which together with exchangeable intercalated cations affects the absorption of water into the interlayer space, and hence controls the layer spacing [37]. These features determine a net negative surface charge for the particle, and in combination with the particle size and the interactions with the screening salt in solution, produce a rich phase behavior in the clay suspensions [38]. A result from laponite suspension by Mourchid et al. is that a line that separates the isotropic and the birefringent gel coincides with the line where the plateau of the osmotic pressure ends up. Recalling the fact that the osmotic plateau starts just at the liquid/solid transition, they proposed a more complete phase diagram exhibiting a pseudobiphilic region with no macroscopic phase separation.

The complexity arises from the several ways in which attractive and repulsive forces act. When van der Waals attraction between the particles is balanced by electrostatic repulsion, particles can remain dispersed, settling only slowly out of solution. Ions from an electrolyte, if present, can screen the repulsive forces between particles and allow them to aggregate together. This aggregation or flocculation may cause the particles to quickly settle out of suspension.

## 1.6 DLVO-theory

### 1.6.1 Attractive Van der Waals and repulsive double layer forces

Individual charged colloid particles dispersed in salt solution interact with each other according to what is commonly and formally known as the DLVO theory. It looks at the balance between two opposing forces, electrostatic repulsion<sup>9</sup> screened by the ions present in the water solution and van der Waals attraction, to explain why some colloidal systems agglomerate while others do not.

A quantitative theoretical analysis of the problem of colloidal stability was independently published in the 1940s by two groups of scientists-Boris Derjaguin and the renowned physicist Lev Landau in the Sovjet Union and Evert Verwey and Theo Overbeek in the

---

<sup>9</sup>The electrostatic part of the DLVO interaction is computed in the mean field approximation. For two spheres of radius  $a$  with constant surface charge  $Z$  separated by a center-to-center distance  $h$  in a fluid of dielectric constant  $\epsilon$  containing a concentration  $n$  of monovalent ions, the electrostatic potential takes the form of a screened-Coulomb or Yukawa repulsion

$$\beta V(h) = Z_B^2 \left( \frac{e^{-\kappa h}}{1 + \kappa a} \right)^2 \frac{e^{-\kappa h}}{h} \quad (1.1)$$

where  $\lambda_B$  is the Bjerrum length,  $\kappa^{-1}$  is the Debye-Hückel screening length, which is given by  $\kappa^2 = 4\pi_B n$  and  $\beta^{-1} = k_B T$  is the thermal energy scale at absolute temperature  $T$ .

Netherlands. This proposed theory became known by the initial letters of their names, DLVO. The Theory assumes that the more long-ranged interparticle interactions mainly control colloidal stability. Two types of forces are considered. A long range London van der Waals force operates irrespective of the chemical nature of the particles or the medium. If the particles are similar, this force is always attractive. Furthermore, most colloidal particles acquire a charge either from surface charge groups or by specific ion adsorption from the solution. For similar particles this charge leads to a repulsive double-layer force. From this the total interaction potential can be written as:

$$V(h) = V_A(h) + V_R(h) \quad (1.2)$$

and the corresponding force will then be

$$F = -\frac{dV}{dh} = -\frac{dV_A}{dh} - \frac{dV_R}{dh} \quad (1.3)$$

A stands for attractive and R repulsive. Depending on the relative strength of the attractive and repulsive terms, the interaction potential can be generated versus distance curves. The interaction potentials have the character of free energies and contain both energetic and entropic contributions.

To illustrate the typical properties of the interaction potentials and the force consider the interaction between two identical half-planes separated by a distance  $h$ . The attractive van der Waals interaction  $V_A$  will here be

$$\frac{V_A(h)}{\text{area}} = -\frac{H_{121}}{12\pi h^2} \quad (1.4)$$

where  $H_{121}$  is the Hamaker constant for medium 1 separated by liquid 2. At large separations, the double-layer interaction force is

$$\frac{F}{\text{area}} \approx 32(kT)^2 \frac{\epsilon_r \epsilon_0}{z^2 e^2} \kappa^2 \Gamma_0^2 e^{-\kappa h} = 64kT c_0^* e^{-\kappa h} \quad (1.5)$$

By integrating this equation the potential is obtained as

$$\frac{V_R(h)}{\text{area}} = \frac{64kT c_0^*}{\kappa} e^{-\kappa h} \quad (1.6)$$

$\Gamma_0$  is defined as  $\tanh(ze\Phi_0/4kT)$  and depends on the potential at the surface, but distance dependence is solely determined by the Debye screening in the solution. From this equation (1.2) can be written

$$\frac{V(h)}{\text{area}} = -\frac{H_{121}}{12\pi h^2} + \frac{64kT c_0^*}{\kappa} e^{-\kappa h} \quad (1.7)$$

and the force

$$\frac{F}{\text{area}} = -\frac{H_{121}}{6\pi h^2} + 64kT c_0^* e^{-\kappa h} \quad (1.8)$$

The attractive term  $V_A(h)$  dominates the repulsive term  $V_R(h)$  when  $h$  is very small. At intermediate separations the double-layer force gives rise to a potential energy barrier if the surface is sufficiently charged and if the electrolyte ions do not screen too much. Figure illustrate the resulting total potential for two choices of  $\kappa$ .

When the low electrolyte concentration makes  $\kappa$  small, substantial energy barrier exists in the total  $V(h)$  and the colloidal system is typically stable. On the hand, for large  $\kappa$  and short screening length  $\kappa^{-1}$ , the barrier is small or nonexistent and the colloidal system is

unstable. To understand the approximate location of the barrier, consider the special case when the barrier is so small that the maximum value of  $V(h)$  is zero. At the maximum

$$\frac{\delta V(h)}{\delta h} = \frac{\delta V_A}{dh} + \frac{\delta V_R}{dh} = 0 \quad (1.9)$$

differentiating equation (1.7) gives

$$\frac{\delta V(h)}{\delta h} = -\kappa V_R - \frac{2}{h} V_A = 0 \quad (1.10)$$

Combined with the condition  $V(h_0) = 0$ , that is,  $V_R = -V_A$ , the separation  $h_0$  at the top of the barrier is obtained as

$$h_0 = \frac{2}{\kappa} \quad (1.11)$$

The barrier moves to larger separations when  $V(h_0) > 0$ , but when the barrier is lower, the colloidal system coagulates rapidly. Thus, as the asymptotic expressions in equations 1.4 and 1.6 are valid for  $h > \kappa^{-1}$ , they are useful for predicting stability or instability.

The van der Waals idealized power-law form for parallel infinitely extended slabs of fixed thickness  $a$  and variable separation  $l$  can be written as

$$\frac{A_{Ham}}{12\pi} \left[ \frac{1}{l^2} - \frac{2}{(l+a)^2} + \frac{1}{l+2a)^2} \right] \quad (1.12)$$

## 1.6.2 The role of salt concentration and aggregation

### 1.6.2.1 Debye screening length

Table 1.1: Roughly values of the Debye's screening lengths for the salt concentrations that are used in the experiment.

Concentration $M$	Debye's screening length $nm$
$10^{-4}$	30
$5 \times 10^{-4}$	13
$10^{-3}$	10
$5 \times 10^{-3}$	4
$5 \times 10^{-2}$	1

The Debye screening length changes strongly with the salt concentration. For a 1-1 electrolyte (e.g NaCl) the screening length is

$$1/\kappa = \frac{0.304}{\sqrt{[NaCl]}} \quad (1.13)$$

Table 1.1 shows the screening length in aqueous solution for the salt concentrations that have been used in the experiment. Therefore, the competition between the repulsive and attractive interactions depends strongly on the added salt. At high salt concentrations the Debye length is smaller than the range of the attractions, and as a result the suspension is unstable and shows irreversible flocculation. A suspension is therefore only stable, when is sufficiently large, meaning that the added salt content has to be sufficiently low. Then the range of the repulsive interactions can easily become larger than the separation between neighboring colloidal particles so that the system becomes highly correlated, although the actual volume occupied by the particles is rather low. In totally pure water at pH 7, the Debye length is 960 nm, or about 1  $\mu m$ .

### 1.6.2.2 Change from stability to instability

In the DLVO theory, colloidal stability is caused by a balance between double-layer repulsion and van der Waals attraction<sup>10</sup>. Therefore, the simplest means of controlling it is to change the nature and concentration of the electrolyte. Experimentally a rather abrupt change from stability to instability on changing the salt concentration will occur. Starting from the DLVO potential and viscosities of the solvent, the expected association rate for any electrolyte concentration can be calculated. A more qualitative approach is to specify a potential  $V(h)$ , which approximately represents the transition from stability to instability in practical terms. A mathematically convenient choice is to set  $V(h)$  equal zero at the barrier maximum. In this case increasing the electrolyte concentration would give an unstable system, or slightly decreasing the electrolyte concentration would achieve long-term stability.

Depending on the electrolyte concentration and surface charge density or potential one of the following may occur:

- a. For highly charged surfaces in dilute electrolyte (long Debye length), there is at the energy barrier a strong long-range repulsion that do a peak at some distance, usually between 1 and 4 nm.
- b. For more concentrated salt solutions there is a secondary minimum (usually beyond 3nm) before the energy barrier. The potential energy minimum at contact is known as the primary minimum. For colloidal system, even though the thermodynamically equilibrium state may be with the particles in contact in the deep primary minimum, the energy barrier may be too high for the particles to overcome during any reasonable time period. When this happens, the particles will either sit in the weaker secondary minimum or remain totally dispersed in the solution. In the latter case the colloid is referred to as being kinetically stable (as opposed to thermodynamically stable).
- c. For surfaces of low charge density or potential, the energy barrier<sup>11</sup> will always be much lower. This leads to slow aggregation, also known as coagulation or flocculation. Above some concentration of electrolyte, known as the critical coagulation concentration, the energy barrier falls below the  $W = 0$  axis and the particles then coagulate rapidly. The colloid is now referred to as being unstable.
- d. As the surface charge or potential approaches zero interaction curve goes to the pure van der Waals curve, and two surfaces now attract each other strongly at all separations (e).

---

<sup>10</sup>The van der Waals effective range typically extends to a few nanometers from the surface of the particles.

<sup>11</sup>If the barrier is cleared, then the net interaction is all attractive, and as a result the particles aggregates.

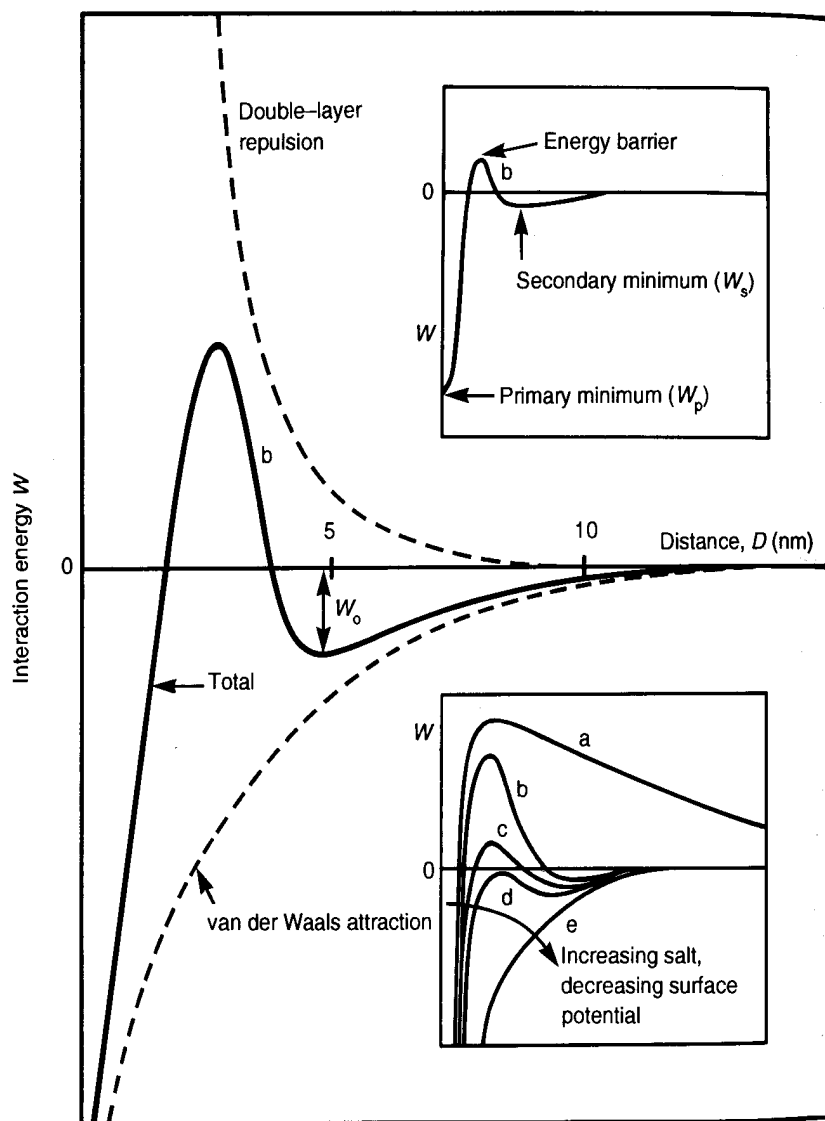


Figure 1.2: Energy versus distance profiles of DLVO interaction. **a.** Surfaces repel strongly; small particles remain stable. **b.** surfaces come into stable equilibrium at secondary minimum if it is deep enough (colloids remain kinetically stable). **c.** Surfaces come into secondary minimum: colloid aggregate slowly. **d.** The critical aggregation concentration. Surfaces may remain secondary minimum or adhere; colloid aggregate rapidly. **e.** Surfaces and colloids coalesce rapidly.

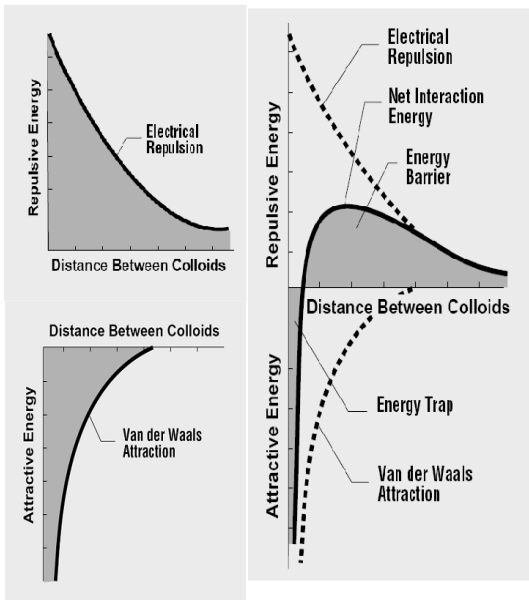


Figure 1.3: To the upper left; Electrostatic Repulsion is always shown as a positive curve. Lower left; Van der Waals Attraction is shown as a negative curve. Right; The net interaction curve is formed by subtraction the attraction curve from the repulsion curve. In the energy trap, the particles can be considered being trapped together by van der Waals forces.

## 1.7 Gels

Attracted particles may join to form extended networks, resulting in gels<sup>12</sup>. In general the particles will have a negative surface charge partly made up for positive charge at the particle edges. This has made suggestions that the particles are connected in a face-to-edge configuration as illustrated in figure 1.1. The result from this is a suggested isotropic "house of cards" structure which has been threatened under many theoretical studies. From a work by Dijkstra et al. [39] the sol-gel transition in a suspension of monodisperse, charged, disklike platelets was examined within a simplified statistical model. The use of an initial primitive model of uniformly charged disks surrounded by microscopic co ions and counterions was reduced to a model of nonintersecting disks carrying a rigid point quadrupole, resulting from the electric double layers around the disks. It was showed that the quadrupolar interactions favored edge-to-face pair configurations which counteract the tendency of parallel nematic alignment of bare disks at high densities. The local structure and phase behavior of the quadrupolar disk model was studied over a broad range of clay concentrations and quadrupole moments which depend on the concentration of added salt by extensive Monte Carlo simulations. The model suspension was found to

<sup>12</sup>A gel (from the lat. gelufreezing, cold, ice or gelatusfrozen, immobile) is a colloidal system in which a porous network of interconnected nanoparticles spans the volume of a liquid medium. In general, gels are apparently solid, jelly-like materials. Both by weight and volume, gels are mostly liquid in composition and thus exhibit densities similar to liquids, however have the structural coherence of a solid. An example of a common gel is edible gelatin. Many gels display thixotropy - they become fluid when agitated, but resolidify when resting.

undergo a reversible sol-gel transition above a critical quadrupolar coupling. The gel phase lacks long-range order, and is reminiscent of a house-of-cards structure in which most of the particles are edge-to-face to each other. The critical concentration and quadrupolar coupling constant are not inconsistent with recent experimental data on the gelation of Laponite suspensions. Since most other recent experimental work has failed to verify the house of cards model, the structural correlations of liquid crystal phases is an alternative model that may be expected in these systems.

## 1.8 Liquid Crystals

The study of liquid crystals began in 1888 when an Austrian botanist named Friedrich Reinitzer observed that a material known as cholestryl benzoate had two distinct melting points. In his experiments, Reinitzer increased the temperature of a solid sample and watched the crystal change into a hazy liquid. As he increased the temperature further, the material changed again into a clear, transparent liquid. Because of this early work, Reinitzer is often credited with discovering a new phase of matter, the liquid crystal phase<sup>13</sup>.

Liquid crystal materials are unique in their properties and uses. As research into this field continues and as new applications are developed, liquid crystals will play an important role in modern technology.

Liquid crystal materials generally have several common characteristics. Among these are a rod-like molecular structure, rigidness of the long axis, and strong dipoles and/or easily polarizable constituents.

The distinguishing characteristic of the liquid crystalline state is the tendency of the molecules (mesogens<sup>14</sup>) to point along a common axis, called the director<sup>15</sup>. This is in contrast to molecules in the liquid phase, which have no intrinsic order. In the solid state, molecules are highly ordered and have little translational freedom. The characteristic orientational order of the liquid crystal state is between the traditional solid and liquid phases and this is the origin of the term mesogenic state, used synonymously with liquid crystal state.

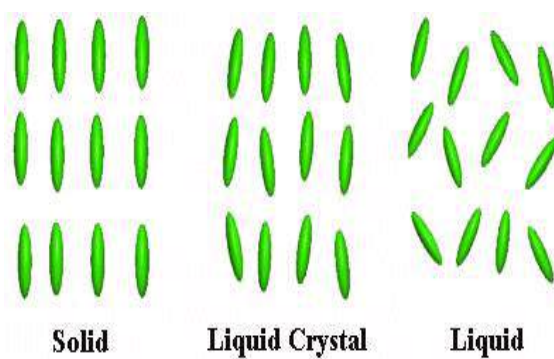


Figure 1.4: The ordering of the crystal phase is placed between the solid and liquid state.

---

<sup>13</sup>a thermodynamic stable phase characterized by anisotropy of properties without the existence of a three-dimensional crystal lattice, generally lying in the temperature range between the solid and isotropic liquid phase, hence the term mesophase.

<sup>14</sup>Rigid rodlike or dislike molecules which are components of liquid crystalline materials.

<sup>15</sup>The molecular direction of preferred orientation in liquid crystalline mesophases.

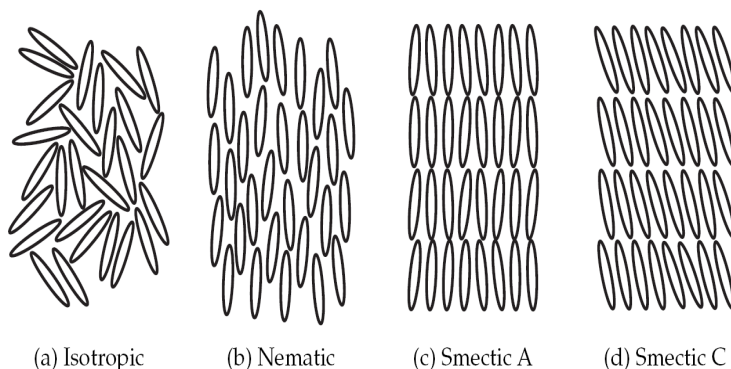


Figure 1.5: The isotropic, nematic, smectic A and smectic C phase of a liquid-crystalline substance.

It is sometimes difficult to determine whether a material is in a crystal or liquid crystal state. Crystalline materials demonstrate long range periodic order in three dimensions. By definition, an isotropic liquid has no orientational order. Substances that are not as ordered as a solid, yet have some degree of alignment, are properly called liquid crystals. To quantify just how much order is present in a material, an order parameter is defined. Traditionally, the order parameter is given as follows:

$$S_2 = \left\langle \frac{3 \cos^2 \theta - 1}{2} \right\rangle \quad (1.14)$$

where  $\theta$  is the angle between the director and the long axis of each molecule. The brackets denote an average over all of the molecules in the sample. In an isotropic liquid, the average of the cosine terms is zero, and therefore the order parameter is equal to zero. For a perfect crystal, the order parameter evaluates to one. Typical values for the order parameter of a liquid crystal range between 0.3 and 0.9, with the exact value a function of temperature, as a result of kinetic molecular motion.

The tendency of the liquid crystal molecules to point along the director leads to anisotropy. This means the properties of a material depends on the direction in which they are measured. The anisotropic nature of liquid crystals is responsible for the unique optical properties exploited by scientists and engineers in a variety of applications.

### 1.8.1 Characterizing Liquid Crystals

The following parameters describe the liquid crystalline structure:

**Positional Order** refers to the extent to which the position of an average molecule or group of molecules shows translational symmetry.

**Orientational Order** represents a measure of the tendency of the molecules to align along the director on a long-range basis.

**Bond Orientational Order** describes a line joining the centers of nearest-neighbor molecules without requiring a regular spacing along that line. Thus, a relatively long-range order with respect to the line of centers but only short range positional order along that line.

Most liquid crystal compounds exhibit polymorphisms, or a condition where more than one phase is observed in the liquid crystalline state. The term mesophase is used to describe the "subphases" of liquid crystal materials. Mesophases are formed by changing the amount of order in the sample, either by imposing order in only one or two dimensions, or by allowing the molecules to have a degree of translational motion. The following section describes the mesophases of liquid crystals in greater detail.

### 1.8.2 Liquid Crystal Phases

The liquid crystal state is a distinct phase of matter observed between the crystalline (solid) and isotropic (liquid) states. There are many types of liquid crystal states, depending upon the amount of order in the material. The ordering of liquid crystalline phases is extensive on the molecular scale. This order extends up to the entire domain size, which may be on the order of micrometres, but usually does not extend to the macroscopic scale as often occurs in classical crystalline solids. However, some techniques (such as the use of boundaries or an applied electric field) can be used to enforce a single ordered domain in a macroscopic liquid crystal sample. The ordering in a liquid crystal might extend along only one dimension, with the material being essentially disordered in the other two directions.

#### 1.8.2.1 Nematic Phases

One of the most common Liquid Crystal phases is the nematic<sup>16</sup>, where the molecules have no positional order, but they do have long-range orientational order. Thus, the molecules flow and their center of mass positions are randomly distributed as in a liquid, but they all point in the same direction (within each domain). Most nematics are uniaxial: they have one axis that is longer and preferred, with the other two being equivalent (can be approximated as cylinders). Some liquid crystals are biaxial nematics, meaning that in addition to orienting their long axis, they also orient along a secondary axis.

Liquid crystals are a phase of matter whose order is intermediate between that of a liquid and that of a crystal. The molecules are typically rod-shaped organic moieties about 25 Ångströms in length and their ordering is a function of temperature. The nematic phase, for example, is characterized by the orientational order of the constituent molecules. The molecular orientation (and hence the material's optical properties) can be controlled with applied electric fields. Nematics are (still) the most commonly used phase in liquid crystal displays (LCDs), with many such devices using the twisted nematic geometry.

#### 1.8.2.2 Smectic phase

The smectic<sup>17</sup> state is another distinct mesophase of liquid crystal substances. Molecules in this phase show a degree of translational order not present in the nematic. In the smectic state, the molecules maintain the general orientational order of nematics, but also tend to align themselves in layers or planes. Motion is restricted to within these planes, and separate planes are observed to flow past each other. The increased order means that the smectic state is more "solid-like" than the nematic. The smectic phases are found

---

<sup>16</sup>The word nematic comes from the Greek  $\nu\eta\mu$  = thread. It refers to thread-like topological defects observed in nematics. They are called 'disclinations'. Hedgehog is the other type of topological defects in nematics.

<sup>17</sup>The name smectic comes from the Greek  $\sigma\mu\gamma\mu$ , which means soap. Friedel found that soap, when mixed with water, also forms a layer-like structure.

at lower temperatures than the nematic, form well-defined layers that can slide over one another like soap. The smectics are thus positionally ordered along one direction. Many compounds are observed to form more than one type of smectic phase. As many as 12 of these variations have been identified, all characterized by different types and degrees of positional and orientational order. In the Smectic A phase, the molecules are oriented along the layer normal, while in the Smectic C phase they are tilted away from the layer normal. These phases are liquid-like within the layers. Smectic phases are more viscous than nematic because of their different nature. In contrast to the case of nematogens, no significant technical use has been found so far for substances in the nematic phase.

### 1.8.2.3 Cholesteric Phases

The cholesteric (or chiral nematic) liquid crystal phase is typically composed of nematic mesogenic molecules containing a chiral center which produces intermolecular forces that favor alignment between molecules at a slight angle to one another. This leads to the formation of a structure which can be visualized as a stack of very thin 2-D nematic-like layers with the director in each layer twisted with respect to those above and below. In this structure, the directors actually form in a continuous helical pattern about the layer normal.

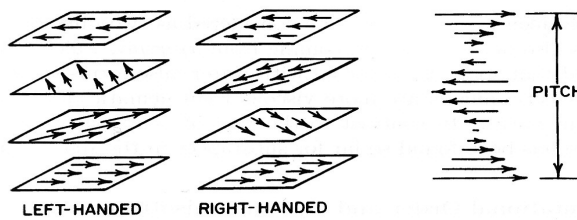


Figure 1.6: The structure of the cholesteric phase. This liquid-crystalline phase in which the director exhibits a periodic twist is formed by chiral nematogens or by dissolving a chiral molecule into a nematic phase. The chirality of the molecule (left or right handed) determines which one of the two senses of rotation is found.

An important characteristic of the cholesteric mesophase is the pitch. The pitch,  $p$ , is defined as the distance it takes for the director to rotate one full turn in the helix as illustrated in figure 1.6. A byproduct of the helical structure of the chiral nematic phase, is its ability to selectively reflect light of wavelengths equal to the pitch length. This leads to striking color phenomena, being selective over the range of frequencies  $f$

$$f = \frac{c_v}{n_{\parallel} p} \rightarrow f = \frac{c_v}{n_{\perp} p} \quad (1.15)$$

where  $c_v$  is the velocity of light in a vacuum,  $n_{\parallel}$  and  $n_{\perp}$  refer to the refractive index parallel and perpendicular to the director. The reflected light is circularly polarised with the same sense of rotation as that of the screw in the chiral-nematic material. This effect can be explained by consider the relevant Maxwell equations. It is then found that a light wave which is circularly polarised in the same sense as the liguid-crystal and has a frequency in the range given by equation (1.15) and a wavevector in the direction of the screw axis cannot propagate through the liquid crystal, it is completely reflected at the surface.

The effect is based on the temperature dependence of the gradual change in director orientation between successive layers, which modifies the pitch length resulting in an alteration of the wavelength of reflected light according to the temperature. The angle at

which the director changes can be made larger, and thus tighten the pitch, by increasing the temperature of the molecules, hence giving them more thermal energy. Similarly, decreasing the temperature of the molecules increases the pitch length of the chiral nematic liquid crystal. This makes it possible to build a liquid crystal thermometer that displays the temperature of its environment by the reflected color. Mixtures of various types of these liquid crystals are often used to create sensors with a wide variety of responses to temperature change. Such sensors are used for thermometers often in the form of heat sensitive films to detect flaws in circuit board connections, fluid flow patterns, condition of batteries, the presence of radiation, or in novelties such as "mood" rings.

In the fabrication of films, since putting chiral nematic liquid crystals directly on a black background would lead to degradation and perhaps contamination, the crystals are micro-encapsulated into particles of very small dimensions. The particles are then treated with a binding material that will contract upon curing so as to flatten the microcapsules and produce the best alignment for brighter colors. An application of a class of chiral nematic liquid crystals which are less temperature sensitive is to create materials such as clothing, dolls, inks and paints.

The wavelength of the reflected light can also be controlled by adjusting the chemical composition, since cholesterics can either consist of exclusively chiral molecules or of nematic molecules with a chiral dopant dispersed throughout. In this case, the dopant concentration is used to adjust the chirality and thus the pitch.

#### 1.8.2.4 Columnar Phases

Columnar liquid crystals are different from the previous types because they are shaped like disks instead of long rods. This mesophase is characterized by stacked columns of molecules, which may be organized into rectangular or hexagonal arrays. The columns are packed together to form a two-dimensional crystalline array. The arrangement of the molecules within the columns and the arrangement of the columns themselves leads to new mesophases. Chiral discotic phases, similar to the chiral nematic phase, are also known.

#### 1.8.3 Electric and Magnetic Field Effects

The response of liquid crystal molecules to an electric field is the major characteristic utilized in industrial applications. The ability of the director to align along an external field is caused by the electric nature of the molecules. Permanent electric dipoles result when one end of a molecule has a net positive charge while the other end has a net negative charge. When an external electric field is applied to the liquid crystal, the dipole molecules tend to orient themselves along the direction of the field. In the following diagram, the black arrows represent the electric field vector and the red arrows show the electric force on the molecule.

Even if a molecule does not form a permanent dipole, it can still be influenced by an electric field. In some cases, the field produces slight re-arrangement of electrons and protons in molecules such that an induced electric dipole results. While not as strong as permanent dipoles, orientation with the external field still occurs.

The effects of magnetic fields on liquid crystal molecules are analogous to electric fields. Because magnetic fields are generated by moving electric charges, permanent magnetic

dipoles are produced by electrons moving about atoms. When a magnetic field is applied, the molecules will tend to align with or against the field.

#### 1.8.4 Chemical Properties of Liquid Crystals

Liquid crystals can be classified into two main categories: thermotropic liquid crystals, and lyotropic liquid crystals. These two types of liquid crystals are distinguished by the mechanisms that drive their self-organization, but they are also similar in many ways.

Thermotropic transactions occur in most liquid crystals, and they are defined by the fact that the transitions to the liquid crystalline state are induced thermally. That is, one can arrive at the liquid crystalline state by raising the temperature of a solid and/or lowering the temperature of a liquid. Thermotropic liquid crystals can be classified into two types: enantiotropic liquid crystals, which can be changed into the liquid crystal state from either lowering the temperature of a liquid or raising of the temperature of a solid, and monotropic liquid crystals, which can only be changed into the liquid crystal state from either an increase in the temperature of a solid or a decrease in the temperature of a liquid, but not both. In general, thermotropic mesophases occur because of anisotropic dispersion forces between the molecules and because of packing interactions.

In contrast to thermotropic mesophases, lyotropic liquid crystal transitions occur with the influence of solvents, not by a change in temperature. Lyotropic mesophases occur as a result of solvent-induced aggregation of the constituent mesogens into micellar structures. Lyotropic mesogens are typically amphiphilic, meaning that they are composed of both lyophilic (solvent-attracting) and lyophobic (solvent-repelling) parts. This causes them to form into micellar structures in the presence of a solvent, since the lyophobic ends will stay together as the lyophilic ends extend outward toward the solution. As the concentration of the solution is increased and the solution is cooled, the micelles increase in size and eventually coalesce. This separates the newly formed liquid crystalline state from the solvent.

A very large number of chemical compounds are known to exhibit one or several liquid crystalline phases. Despite significant differences in chemical composition, these molecules have some common features in chemical and physical properties. There are two types of thermotropic liquid crystals: discotics and rod-shaped molecules. Discotics are flat disc-like molecules consisting of a core of adjacent aromatic rings. This allows for two dimensional columnar ordering. Rod-shaped molecules have an elongated, anisotropic geometry which allows for preferential alignment along one spatial direction.

#### 1.8.5 Light and Polarization

Light can be represented as a transverse electromagnetic wave made up of mutually perpendicular, fluctuating electric and magnetic fields.

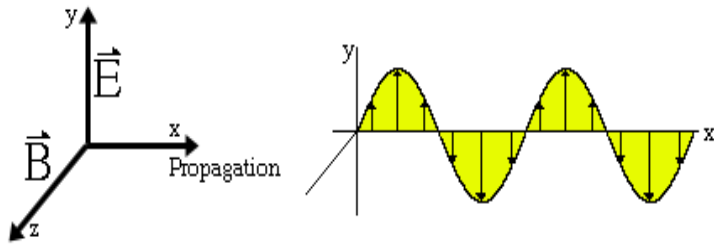


Figure 1.7: The left side shows the electric field in the xy plane, the magnetic field in the xz plane and the propagation of the wave in the x direction. The right half shows a line tracing out the electric field vector as it propagates. Since the two component is essentially the same, only the electric field vector is being dealt with.

Ordinary white light is made up of waves that fluctuate at all possible angles. Light is considered to be linearly polarized when it contains waves that only fluctuate in one specific plane. The wave can move up and down, but motion is blocked in any other direction. A polarizer is a material that allows only light with a specific angle of vibration to pass through. The direction of fluctuation passed by the polarizer is called the "easy" axis.

If two polarizers are set up in series so that their optical axes are parallel, light passes through both. However, if the axes are set up 90 degrees apart (crossed), the polarized light from the first is extinguished by the second. As the angle rotates from 0 to 90 degrees, the amount of light that is transmitted decreases. This effect is illustrated in figure 1.8.

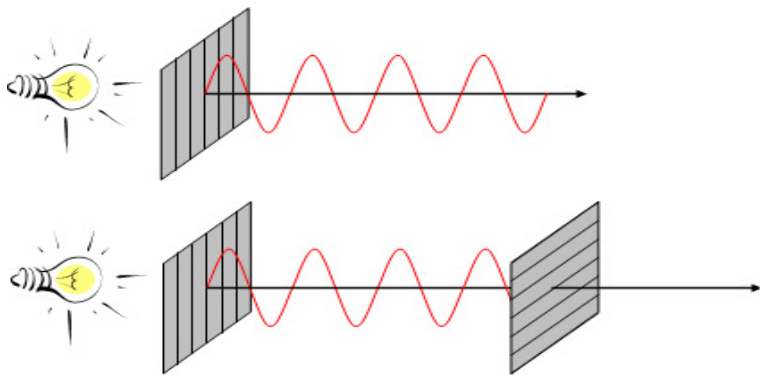


Figure 1.8: Polarizer with vertical transmission axis. Crossed polarizers will block out the light.

Linear polarization is merely a special case of circularly polarized light<sup>18</sup>. Consider two light waves, one polarized in the YZ plane and the other in the XY plane. If the waves reach their maximum and minimum points at the same time (they are in phase), their vector sum leads to one wave, linearly polarized at 45 degrees. This is shown in figure 1.9.

---

<sup>18</sup>A condition caused by two waves whose electric field components are 90 degrees out of phase, causing an effective rotation of the electric field about an axis in direction of propagation.

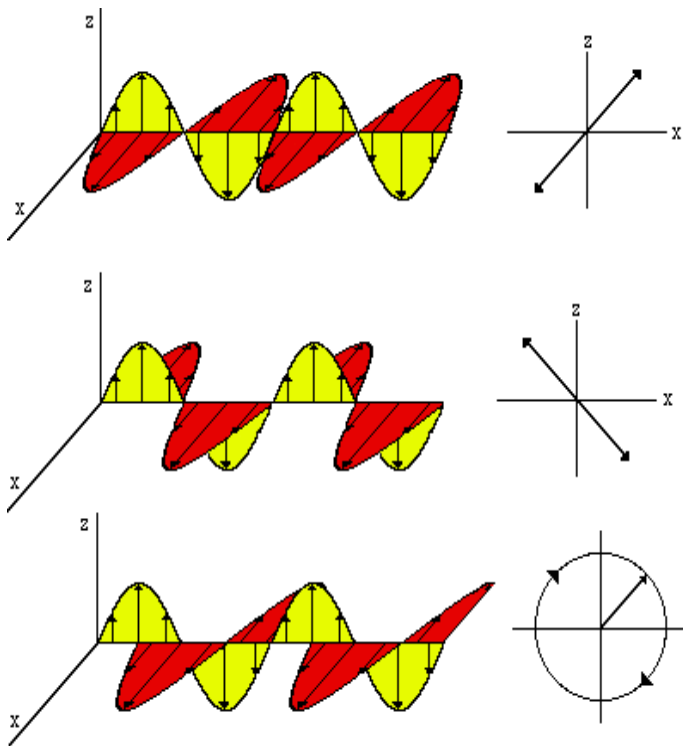


Figure 1.9: From top: Linearly polarized at 45 degrees, linearly polarized at 45 degrees in the opposite sense and circularly polarized light.

Similarly, if the two waves are 180 degrees out of phase, the resultant is linearly polarized at 45 degrees in the opposite sense.

If the two waves are 90 degrees out of phase (one is at an extremum and the other is at zero), the resulting wave is circularly polarized. In effect, the resultant electric field vector from the sum of the components rotates around the origin as the wave propagates. Figure 1.9 shows the sum of the electric field vectors for two such waves.

The most general case is when the phase difference is at an arbitrary angle (not necessarily 90 or 180 degrees.) This is called elliptical polarization because the electric field vector traces out an ellipse (instead of a line or circle as before).

#### 1.8.5.1 Birefringence in Liquid Crystals

Liquid crystals are found to be birefringent, due to their anisotropic nature. That is, they demonstrate double refraction (having two indices of refraction). Light polarized parallel to the director has a different index of refraction (that is to say it travels at a different velocity) than light polarized perpendicular to the director.

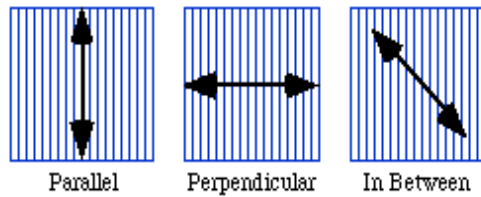


Figure 1.10: The lines represent the director field and the arrows show the polarization vector.

When light enters a birefringent material, such as a nematic liquid crystal sample, the process is modeled in terms of the light being broken up into the fast (called the ordinary ray) and slow (called the extraordinary ray) components. Because the two components travel at different velocities, the waves get out of phase. When the rays are recombined as they exit the birefringent material, the polarization state has changed because of this phase difference. Light traveling through a birefringent medium will take one of two paths depending on its polarization.

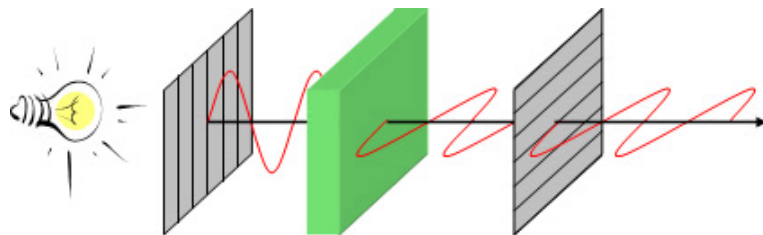


Figure 1.11: A liquid crystal layer between crossed polarizers can change the polarization of the light propagating through, which results in light transmission after the crossed polarizers.

The birefringence of a material is characterized by the difference,  $\Delta n$  which is proportional to the nematic order parameter, in the indices of refraction for the ordinary and extraordinary rays. Since the index of refraction of a material is defined as the ratio of the speed of light in a vacuum to that in the material, the following equation holds for this case:

$$|| =$$

The length of the sample is another important parameter because the phase shift accumulates as long as the light propagates in the birefringent material. Any polarization state can be produced with the right combination of the birefringence and length parameters.

It is convenient here to introduce the concept of optical path in media since for the above two wave components traveling with different speeds in a birefringent material, the difference in optical paths will lead to a change in the polarization state of the wave as it progresses through the medium. By defining the optical path for a wave traveling a distance  $L$  in a crystal as  $nL$  so that the optical path difference for the two wave components mentioned above will be  $L(n_{||} - n_{\perp}) = L\Delta n$ . The resultant phase difference between the two components (the amount by which the slow, extraordinary component lags behind the fast, ordinary one) is just  $2\pi L\Delta n / \lambda_v$  where  $\lambda_v$  is the wavelength in vacuum. The size of the phase shift determines the intensity of the transmitted light.

### 1.8.5.2 Application to Polarized Light Studies of Liquid Crystals

Consider the case where a liquid crystal sample is placed between crossed polarizers whose transmission axes are aligned at some angle between the fast and slow direction of the material. Because of the birefringent nature of the sample, the incoming linearly polarized light becomes elliptically polarized. When this ray reaches the second polarizer, there is now a component that can pass through, and the region appears bright. For monochromatic light, the magnitude of the phase difference is determined by the length and the birefringence of the material. If the sample is very thin, the ordinary and extraordinary components do not get very far out of phase. Likewise, if the sample is thick, the phase difference can be large. If the phase difference equals 360 degrees, the wave returns to its original polarization state and is blocked by the second polarizer. The size of the phase shift determines the intensity of the transmitted light.

If the transmission axis of the first polarizer is parallel to either the ordinary or extraordinary directions, the light is not broken up into components, and no change in the polarization state occurs. In this case, there is not a transmitted component and the region appears dark.

In a typical liquid crystal, the birefringence and length are not constant over the entire sample. This means that some areas appear light and others appear dark. The light and dark areas that denote regions of differing director orientation, birefringence, and length.

The Schlieren texture, as this particular arrangement is known, is characteristic of the nematic phase. The dark regions that represent alignment parallel or perpendicular to the director are called brushes. The next section will describe the textures of liquid crystals in greater detail, but before going there lets see how birefringence can lead to multicolored images in the examination of liquid crystals under polarized white light.

### 1.8.5.3 Colors Arising From Polarized Light Studies

Birefringence can lead to multicolored images in the examination of liquid crystals under polarized white light. Examples of retarding plates in the sample can be used in understanding the origin such observed colors. They are designed for a specific wavelength and thus will produce the desired results for a relatively narrow band of wavelengths around that particular value. If, for example, a full-wave plate designed for wavelength is  $\lambda$ , is placed between crossed polarizers at some arbitrary orientation and the combination illuminated by white light, the wavelength  $\lambda$  will not be affected by the retarder and so will be extinguished (absorbed) by the analyzer. However, all other wavelengths will experience some retardation and emerge from the full-wave plate in a variety of polarization states. The components of this light passed by the analyzer will then form the complementary color to  $\lambda$ .

### 1.8.5.4 Temperature Dependence of Birefringence

Since the birefringence of a material results from its anisotropy and the anisotropy of liquid crystals show a strong temperature dependence, vanishing at the nematic to isotropic phase transition, the birefringence shows a significant temperature dependence. The measurement of the temperature dependence of the birefringence of a liquid crystal material in the nematic phase is instructive for a variety of reasons. It provides a reminder of the consequences of birefringence in liquid crystals as well as emphasizing the corresponding temperature dependence of the order parameter and it introduces some of the concepts and experimental methods of birefringence measurements.

### 1.8.5.5 Liquid Crystal Textures

The term texture refers to the orientation of liquid crystal molecules in the vicinity of a surface. Each liquid crystal mesophase can form its own characteristic textures, which are useful in identification.

If mesogenic materials are confined between closely spaced plates with rubbed surfaces and oriented with rubbing directions parallel, the entire liquid crystal sample can be oriented in a planar texture, as shown in figure 1.12. Mesogens can also be oriented normal to a surface with the use of appropriate polymer films, or in the presence of an electric field applied normal to the surface, giving rise to the homeotropic texture.

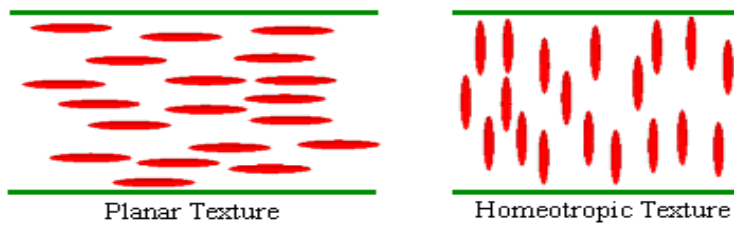


Figure 1.12: Planar(left) and Homeotropic(right) textures

### 1.8.6 Isotropic-nematic transition

Computer simulations of Eppenga and Frenkel [40] has shown that in plate colloid systems, a transition from an isotropic to a nematic phase is expected at a critical particle density. Many molecular fluids consisting of anisometric molecules exhibit one or several liquid crystalline phases between the usual isotropic liquid phase and the solid phase [41]. The nematic, characterized by short range translational, and long range orientational order, is simplest among these liquid crystalline phases. Whether or not a given molecular liquid will have a nematic phase depends in a rather subtle way on the shape of the constituent molecules. First of all the intermolecular interactions have to be sufficiently anisotropic to favor orientational ordering. However, most non-spherical molecules freeze before they can form a liquid crystal. Therefore a good model for a nematogen must satisfy two conditions; first, it must be sufficiently anisotropic to favor orientational order, and second, at the temperature and density of the isotropic-nematic transition the solid phase should still be thermodynamically unstable. Two distinct molecular properties may help to favor the nematic phase over the solid. The first is the presence of internal degrees of freedom which contribute to the entropy in the liquid phase but are frozen out in the solid. Most thermotropic liquid crystal belong to this category. The second possibility is that the average excluded volume of a pair of randomly oriented molecules is much larger than the volume occupied by these molecules in a close packed crystal. In this case the density at which orientational ordering becomes favorable is much lower than the freezing density. Many lyotropic liquid crystals fit this description. Most models for nematic ordering either belong to the latter category (the Onsager theory [42] is the outstanding example) or ignore the possibility of freezing altogether (this is true for the Maier-Saupe theory [43] as well as for many of the applications of scaled particle theory [44], [45]).

A consideration of a model fluid consisting of infinitely thin hard platelets cannot crystallize at any finite density because such infinitely thin discs have zero volume. Yet as two non-parallel discs have a finite excluded volume, orientational ordering can, and in fact must, occur at a finite density. The hard-platelet system can therefore be expected to exhibit an isotropic phase at low densities and a nematic phase at high densities.

No other phases of the hardplatelet system are to be expected. It is for this reason that hard-platelets constitute a very clean model system to study the isotropic-nematic transition. There are several questions related to the isotropic-nematic transition which make a numerical study of this model system interesting. The first question is related to the role of repulsive forces in driving the I-N transition. Whereas there is general consensus that the structure of simple liquids is almost exclusively determined by the strong repulsive forces that act between atoms at short distances [46], the situation is less clear in the case of liquid crystals. There are two distinct theoretical approaches to the description of the I-N transition based on almost diametrically opposed points of view. On the one hand there is the Maier-Saupe theory, a mean-field description which never considers the effect of harsh repulsive forces on the liquid structure explicitly. In the Maier-Saupe theory the onset of nematic ordering is attributed to the effect of relatively long-ranged anisotropic intermolecular interactions <sup>19</sup>. The Maier-Saupe theory yields a qualitatively correct description of a number of properties of nematic liquid crystals [47], but the assumption that harsh repulsive forces are irrelevant is hard to justify. However, pointed out by Sluckin and Shukla [48] that the main results of the Maier-Saupe theory can be rederived without such an assumption, but at a cost: the simple relation between molecular field and intermolecular potential is replaced by a much more complicated one. On the other hand there are several theoretical approaches which start out from the assumption that the effect of the anisotropic repulsive forces on the liquid structure is of crucial importance for the transition to the nematic phase. Oldest among these is Onsager's theory for the I-N transition of a system of thin hard rods. The Onsager theory predicts that such a system will exhibit a very strong first order isotropic-nematic transition. This may be correct for thin rods but it is certainly of little relevance for typical thermotropic liquid crystals which have a very weak I-N transition. Scaled particle theories seem somewhat better suited to describe the onset of nematic ordering in fluids of harshly repulsive particles with realistic length-to-width ratios. There is, however, a conspicuous scarcity of numerical data on the equation of state of hard, non-spherical convex bodies to which the scaled particle predictions can be compared. In the few cases where a direct comparison has been made, [49, 50], the predictions of scaled particle theory are found to deviate by at most 20 percent (and often much less) from numerical data.

### 1.8.7 Applications of liquid crystals

Liquid crystals find wide use in liquid crystal displays, which rely on the optical properties of certain liquid crystalline molecules in the presence or absence of an electric field. In a typical device, a liquid crystal layer sits between two polarizers that are crossed. The liquid crystal is chosen so that its relaxed phase is a twisted one. This twisted phase reorients light that has passed through the first polarizer, allowing it to be transmitted through the second polarizer and reflected back to the observer. The device thus appears clear. When an electric field is applied to the LC layer, all the mesogens align (and are no longer twisting). In this aligned state, the mesogens do not reorient light, so the light polarized at the first polarizer is absorbed at the second polarizer, and the entire device appears dark. In this way, the electric field can be used to make a pixel switch between clear or dark on command. Color LCD systems use the same technique, with color filters used to generate red, green, and blue pixels. Similar principles can be used to make other liquid crystal based optical devices.

Thermotropic chiral LCs whose pitch varies strongly with temperature can be used as crude thermometers, since the color of the material will change as the pitch is changed.

---

<sup>19</sup>(e.g. the anisotropic dispersion forces which decay as  $r^{-6}$ )

Liquid crystal color transitions are used on many aquarium and pool thermometers. Other liquid crystal materials change color when stretched or stressed. Thus, liquid crystal sheets are often used in industry to look for hot spots, map heat flow, measure stress distribution patterns, and so on. Liquid crystal in fluid form is used to detect electrically generated hot spots for failure analysis in the semiconductor industry. Liquid crystal memory units with extensive capacity were used in Space Shuttle navigation equipment.

It is also worth noting that many common fluids are in fact liquid crystals. Soap, for instance, is a liquid crystal, and forms a variety of LC phases depending on its concentration in water.

# Chapter 2

# Experiment

The idea is to collect visually information about the aqueous clay suspension as the particles is settling under gravity. The different phases should be distincted and recorded as they are evolving in time. Since time and the ability to see small details in the sample are important factors in such an experiment, the main gear is a high resolution digital camera with an built in automaticly timer control. The high number of pictures taken can easily be sat under further analysis by lining different shots for comparisons, zoom functions for details or video making tools for continuous dynamics.

## 2.1 Na-Fluorohectorite powder preparations

For the experiment two different Na-fluorohectorite powder preparations<sup>1</sup> is used. The first powder were prepared finished in April 2006 and a newer preparation in August 2006. These two types of Na-FH powder is by this refered to as april and august powder respectively. After the dried up process, both of the powders were with some degree crushed by a mechanical crusher (IKA A11 basic, Guangzhou, China). For samples both powders is used by no further preparations. Further crushing was done by mortel (Haldenwanger) to obtain a very fine crushed powder. This powder was wighted and solved in salt solution by hand shaking.

## 2.2 Vitrotube

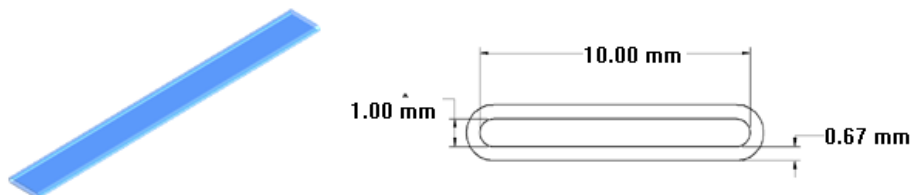


Figure 2.1: The vitrotube with inner dimension of 1.00 x 10.00 mm and wall thickness of 0.67 mm.

The sample containers that is used for the experiment are of type Vitrotube 4410-100 from VitroCom (formerly known as VitroDynamics, USA). The containers are a 100 mm high

<sup>1</sup>Ion exchanged through dialysis by Ahmed Gmira

synthetic fused silica glass tube with inner dimensions of 1x10 mm and wall thickness of 0.67 mm. The tubes have open ends that need to be sealed before and after injection. The glass tubes should not be retained by fusing, since this affect the polarizing abilities to the glass. Alternative retaining were done by using silicon rubber of type ELASTOSIL A33. This glue will by proper use manage to seal the tube, but should not be used since some of the silicone at the bottom seem to interact with the liquid sample. By some early samples, Capillary Wax (Hampton Research HR4-328) was used to seal the upper part of the tube. This was hardly used because of both the time consuming process and the fact that the wax can have a bad habit to "pop out" of the containers. The sampletubes are at both ends sealed by Parafilm (PM-992) a laboratory film from SPI Supplies and Structure Probe, Inc. Without to much investigations, this film does not seem to do any harm to the sample.

## 2.3 Polarizers

For the setup two types of polarizers from Edmund Optics is used. The polarizer that is behind the sample is a commercial-quality film polarizers with 22% transmission. The polarization efficiency<sup>2</sup> is over 99%. The film is coated with a peel-off protective layer for safe, easy handling.

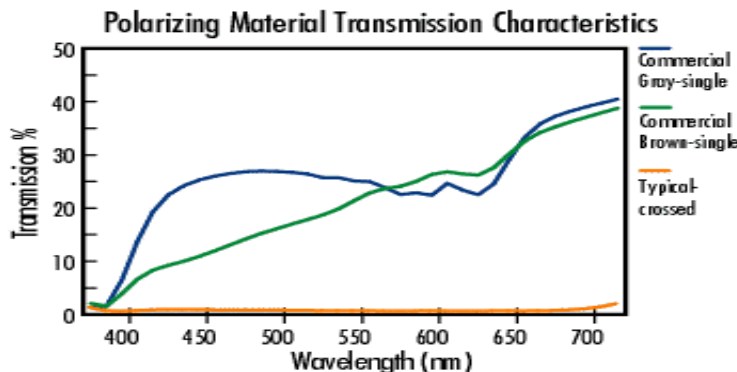


Figure 2.2: Polarizing material transmission characteristics for the film polarizer.

The polarizer used before the camera is a mounted linear glass standard 42 mm threaded polarizing filter. Mounted clear aperture is mount diameter less 5mm and mounted maximum outer diameter is mount diameter plus 2mm. The thickness of the filter includes 2mm male thread. The filter has a polarization efficiency of 95%, single transmission of 30% and 0.15% average transission when crossed.

---

<sup>2</sup>Polarization Efficiency is the percentage of how efficiently one polarizer polarizes incident light over the total amount of polarized light. With 99% efficiency the polarizer transmits 99% of the incident light in the intended polarization (p-polarization state) and 1% in the opposite polarization (s-polarization state). Polarizaton Efficiency = P.E. (%) =  $[(H_0 - H_{90}) / (H_0 + H_{90})]^{1/2} \times 100$ , where  $H_0$  is the average transmittance (unpolarized incident light) of parallel polarizers and, and  $H_{90}$  is the average transmittance of crossed polarizers, over 400-700nm. (Handbook of Optics (Vol. I, 5-13))

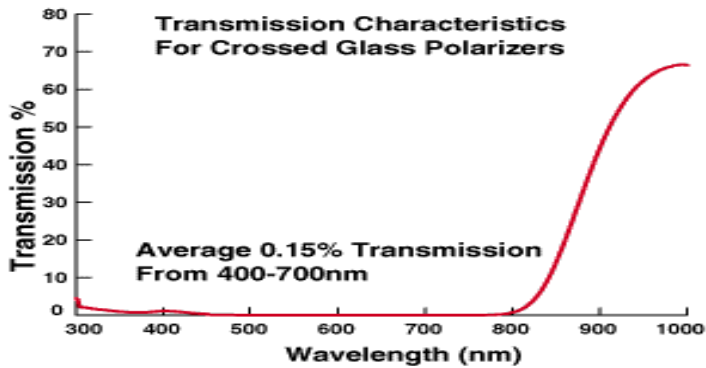


Figure 2.3: Polarizing material transmission characteristics for the linear glass filter polarizer.

## 2.4 Canon EOS 350D

### Features

- 8.0 MP
- 3 fps with up to 14 image burst
- E-TTL II flash system
- DIGIC II
- 7-point AF
- DPP RAW image processing software
- Separate RAW/JPEG image recording
- USB 2.0 Hi-speed/Video Out
- Compatible with EF/EF-S lenses/EX Speedlite flashes
- PictBridge compatible

**Quality** The EOS 350D Digital employs Canon's CMOS technology, for images with 8.0 Megapixel resolution. The camera can take shot with responsive 3 frame per second, 14 frame burst performance and instant 0.2 second start up time. DIGIC II architecture taken from Canon's pro-series cameras ensures no compromise, effective and fast image processing.

**Focus** With 7 auto focus points distributed across the frame, the camera gives accurate focusing, even with off-centre subjects. The focus can be locked before the shot with One Shot AF, or to AI Servo AF. The focus is fine tuned once at manual focus. Automatic focus may not give the most accurate focus when focused at the samples.

**Lenses** The EOS 350D Digital is compatible with more than 60 Canon EF lenses, including Canon's EF-S lenses.

**Connectivity** A USB 2.0 Hi-Speed interface ensures rapid image uploads. The EOS 350D Digital takes both CF and CF-II cards, including cards of over 2GB capacity.

The camera can be put into a lot of different modes, depending of the use. For pictures taken for this experiment, the  $Tv^3$  shutter-priority AE mode has been used. In this mode the shutter speed can set, and the camera will automatically sets the aperture value to suit the subjects's brightness. This is called shutter-priority AE.

## 2.5 Experimental Setup

### 2.5.1 Cardboard setup

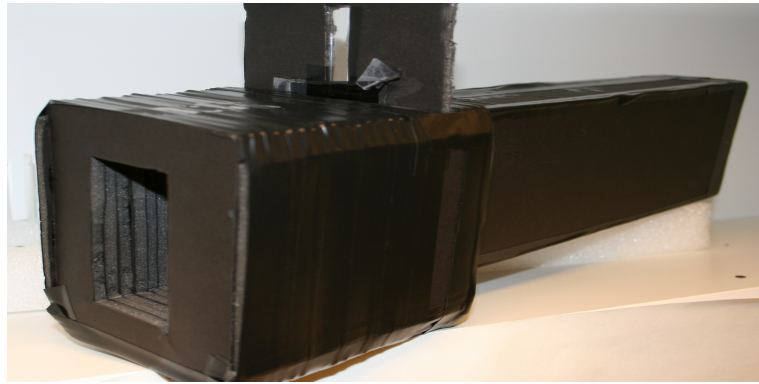


Figure 2.4: Old setup made out of cardboard.

In the start up of the project a simple cardboard holderbox, made by Davi, was used as the setup for the samples. Three samples was in all tested out with this setup. The box did a great job in isolating the samples from outer lights, but was layed down because the samples repositioned after a samplechange and it could only hold one sample at a time. The box also suffered from shadows effect in the lower and upper part of the sample and it could only cover two-third of the whole sample tube.

---

<sup>3</sup>Tv stands for time value

### 2.5.2 Metal stage setup



Figure 2.5: The stage upside down attached to a metal board. The board has holes through the centre line to fastened the camera and polarizers. The camera is placed about 20 cm from the samples. From behind the samples, there are two layers of polarizing films.

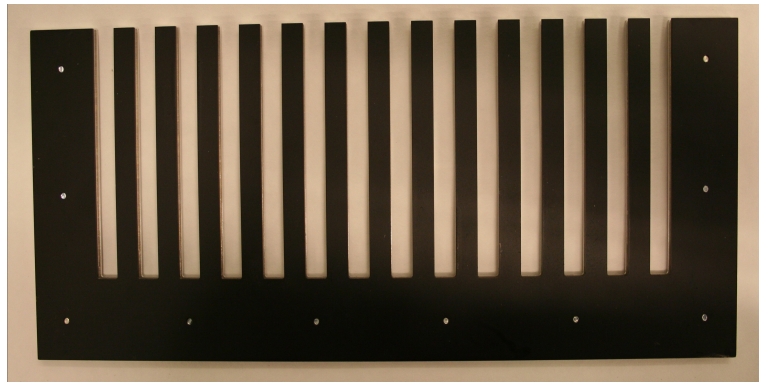


Figure 2.6: The rack can hold up to 14 samples. It is designed for the purpose to use vitrotubes with parafilm stucked around the ends.

To make a stable system that could hold several samples for fast recording, a stage setup with a metal holder was worked out. A metric long travel linear translation stage and track from Edmund Optics makes up the fundament of the breadboard traveling. The track is made from extruded aluminum into a low-profile dovetail design to fit against the mating dovetail of the mounting stage. Helical movement on brass rack allows for precision and smooth travel along the entire length of track. Each track includes a scale that is aligned with the stage vernier. The coarse movement of the stage can be aligned within 0.1 mm. Combination of stage and track has total height of 40 mm; knobs do not exceed stage height. The total length of the stage is 250 mm and is put upside down for the experimental purpose. On top of the stage, sample tube racks is placed between to double

pillars. The rack is designed with the vitrotube 4410-100 in mind. Drawings of the racks can be found in appendix B. It is composed of 3 parts, where a middle part is surrounded on both sides with two equal fronts. The first rack that was made has a slightly smaller slit width than the later version. The tube width were made larger because is should make a better fit for vitrotubes sealed with parafilm. The racks can hold a number of 12 and 14 samples for the two versions respectively. The part of the rack heading towards the camera is painted black to reduce reflection. The three parts of the rack is fastened with even distributed screws across the the middle line of the outer parts.

## 2.6 UVP white light transilluminator

The light source that is being used for illuminations is a white light transilluminator (UVP, Inc. Upland, CA USA) model TW-43, fuse: 2 x T2 ampere. The light does not get hot when burning for a long time, but illumination of the samples for some longer period give them a greenish look. Since the light is constantly burning, all samples except some older ones, have this dull green color.



Figure 2.7: UVP White Light Transilluminator

## 2.7 Magnet

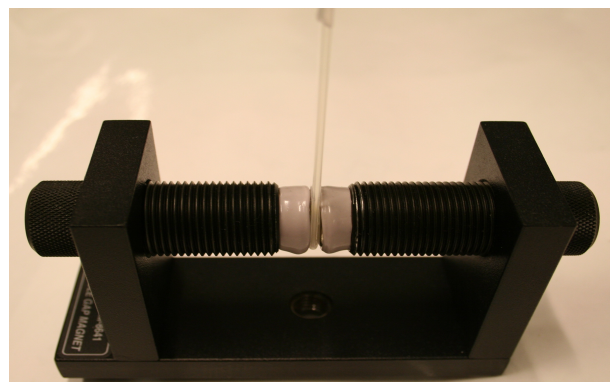


Figure 2.8: It is small, but the magnetic field strength goes up to 1 Tesla when the gaps are screwed this much together.

For studies of the magnetic effect of the clay suspension, a variable gap lab magnet from Pasco scientific is used. The variable Gap Lab Magnet consists of two 19 mm diameter neodymium magnets on an iron base, that are plastic-coated to prevent chipping. The magnets heavy-duty iron base is stable in four different freestanding positions and also mounts on standard 12.7 mm rods. The magnet will not have a great effect on its surroundings because the field drops off to about 30 Gauss at the outside edges of the magnet. The maximum magnetic field strength is from the manufacture given to be 0.75 Tesla, however with over screwing to a minimum gap of 2.2 mm a magnetic field strength of nearly 1 Tesla has been measured. With this gap, a clay suspension sample in a vitrotube will at least in the central part experience a magnetic field of this strength.

## 2.8 Weighing of different phases

For two samples, april and august, the different phases were weighed up. The samples were made in syringes where the top had been cut off. The idea by this is to take off a very small amount of the top part, and set this to vaporization. When the water have vaporized, the dry clay drop can be weighed up. By pressing up the syringe, the next phase will reach the top for take off and new measurement. The samples were weighed up by always taking an equal amount from the top. This resulted in a total of 180 measurepoints for each sample.

## 2.9 Computer softwares

When taking pictures, the Canon software ZoomBrowser EX is used for direct view of the pictures. Canon's PhotoStudio 5.5 is used for further treatment of the pictures. Movies made from the jpg pictures, has been created by the audio/video editing, converter program Blaze Media (Mystik Media). This program allows you to make movies of MPEG-1, MPEG-2, AVI, WMV, ASF, MOV formats. For further video editing, as putting on the time frame on the videos, Ulead MediaStudio Pro 8.0 is used.

# Chapter 3

## Results and Discussion

### 3.1 Sample distribution

Divided on 36 different samples the total number of shots taken with the camera amounts to around 11 700 pictures. Figure 3.1 shows all the samples distributed over NaCl concentration and weight % with their powder type and its crushing property. In addition to these samples listened, two extra samples has been sat between the gap magnet right after they were made. 3 % april was exposed for the 1 Tesla magnetic field in 13 days, and the result in this report for 1% august is for 10 days settling. As an additional experiment, two samples of both powder type were with a  $3\% 10^{-3}$  weight concentration, made in a 50 ml cutted syringe. The weight distibution through the sample is plotted for height (volum) versus measured weight.

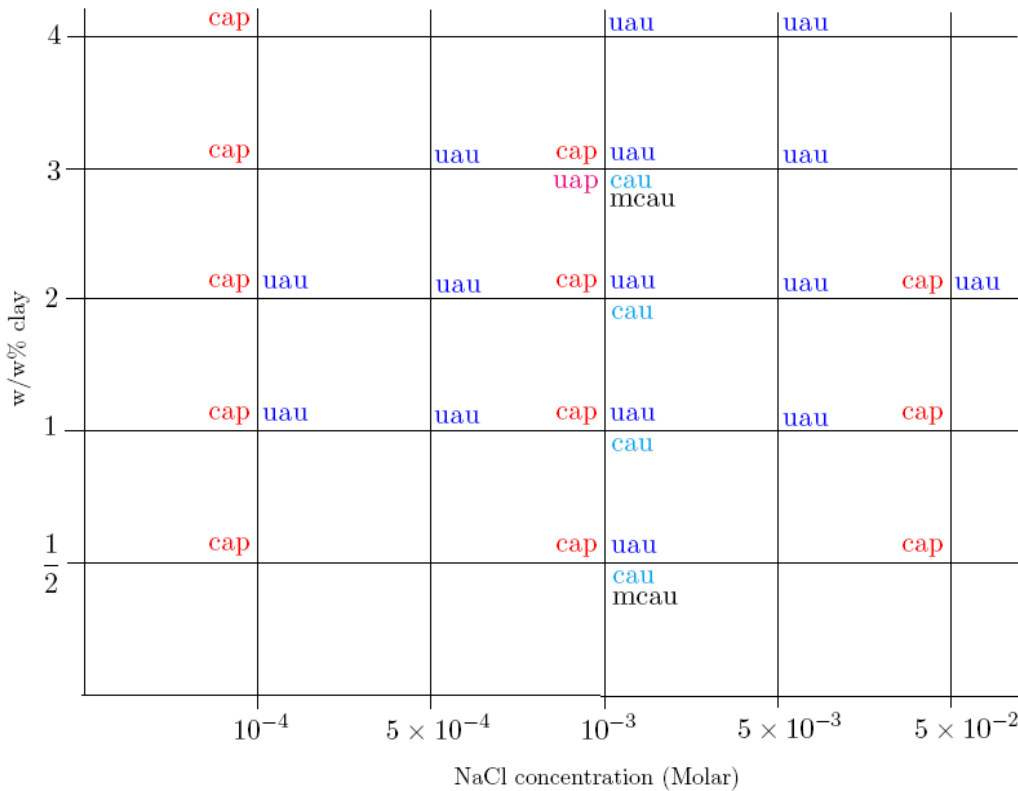


Figure 3.1: The various samples how they have been made by different weight % in salt solutions ranging from  $10^{-4}$  to  $5 \times 10^{-2}$  Molar. **cap** is crushed april powder, **uau** is uncrushed august powder, **cau** is crushed august powder, **uap** is uncrushed april powder and **mcau** is august powder that have been extra crushed with a mechanical crusher.

### 3.2 Comparison across concentrations

Figures 3.2 and 3.3 shows the longest gravity settling process for samples of 2 weight % for the different august and april fluorohectorite powder. For both powder types it is clear that low concentration gives higer suspension hight. The results are in typical accordance with Debye's screening lenght for a qualitative regard. For the  $5 \times 10^{-2}$  M high concentrated samples the clay aggregates very fast to a stable condition, where it stucks in the tube and furhter settling stops up. The April powder differ from the the August powder by not having a layer of heavy sediment at the bottom. This difference is very recognizable when looking at the first minutes after the samples have been filled in the tube. This is mainly due to the fact that the april powder has undergone the extensive mortel crushing.

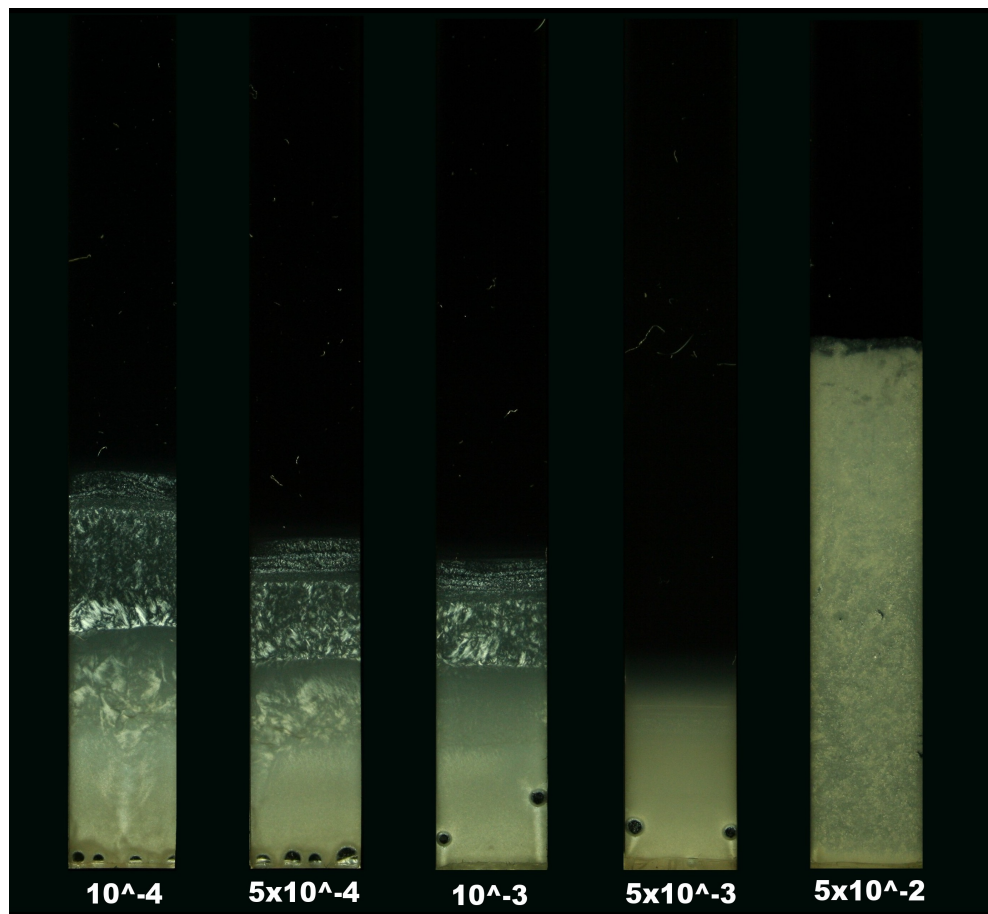


Figure 3.2: 2 w/w% uncrushed august with salt concentration from  $10^{-4}$  to  $5 \times 10^{-2}$ . The three samples with lowest concentration have an age of 50 days, while the sample with concentration  $5 \times 10^{-3}$  is 12 days old. The  $5 \times 10^{-2}$  Molar sample stopped from further evolvement after 1 day. The  $10^{-4}$  M and  $5 \times 10^{-4}$  M samples differ from the  $10^{-3}$  by having a much more muddy appereance in the middle phase. As can be seen by the movies of the these two samples, this distinction is at least to some extent caused by air bubbles advancing to the surface.

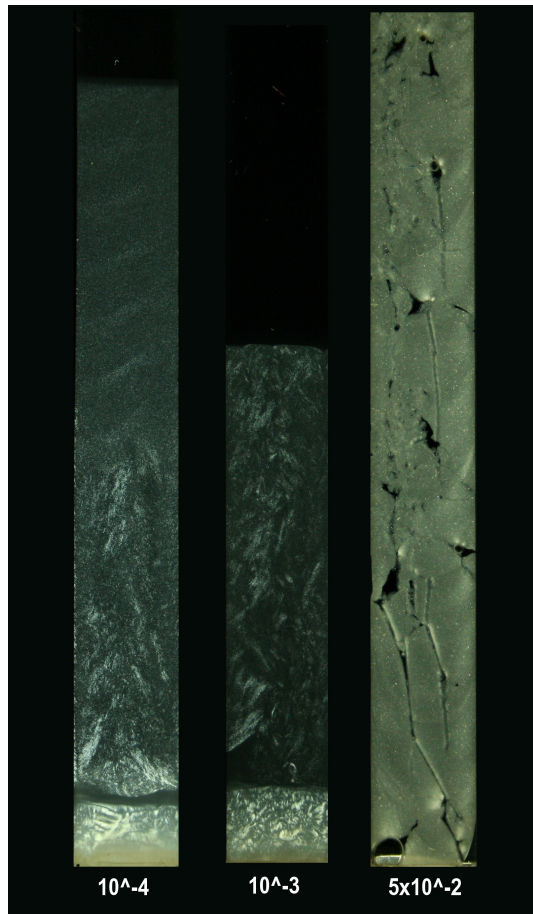


Figure 3.3: 2 w/w% crushed april with salt concentration  $10^{-4}$  (16 days),  $10^{-3}$  (36 days) and  $5 \times 10^{-2}$  (69 days). The 69 days time elapsed means very little to the heigh concentrated  $5 \times 10^{-2}$  sample, since it looks almost identical as it did after its first 5-6 days from sample preparation. For the two samples with lowest concentration the lowest parts seems to be of nematic character. The  $10^{-4}$  sample have a more darker slit above the bottom birefringence part. This slit could seem to play a role as a rest foundation for the clay particles located above. These particles sure show birefringence of the same kind as the bottom part, but do not form up the same kind of a distinct layer. Instead, the birefringence is spread up through the tube in a fortuitous way. This same fluctuation is also characteristic for the ten times higher concentrated  $10^{-3}$  sample, but here there is no sign for any intermediary dark slit. By looking at the movies for these two samples, the fluctuating particles move in a downward gravity fluided way for the  $10^{-4}$  sample, but have a much more all directed dynamic movement for the  $10^{-3}$ .

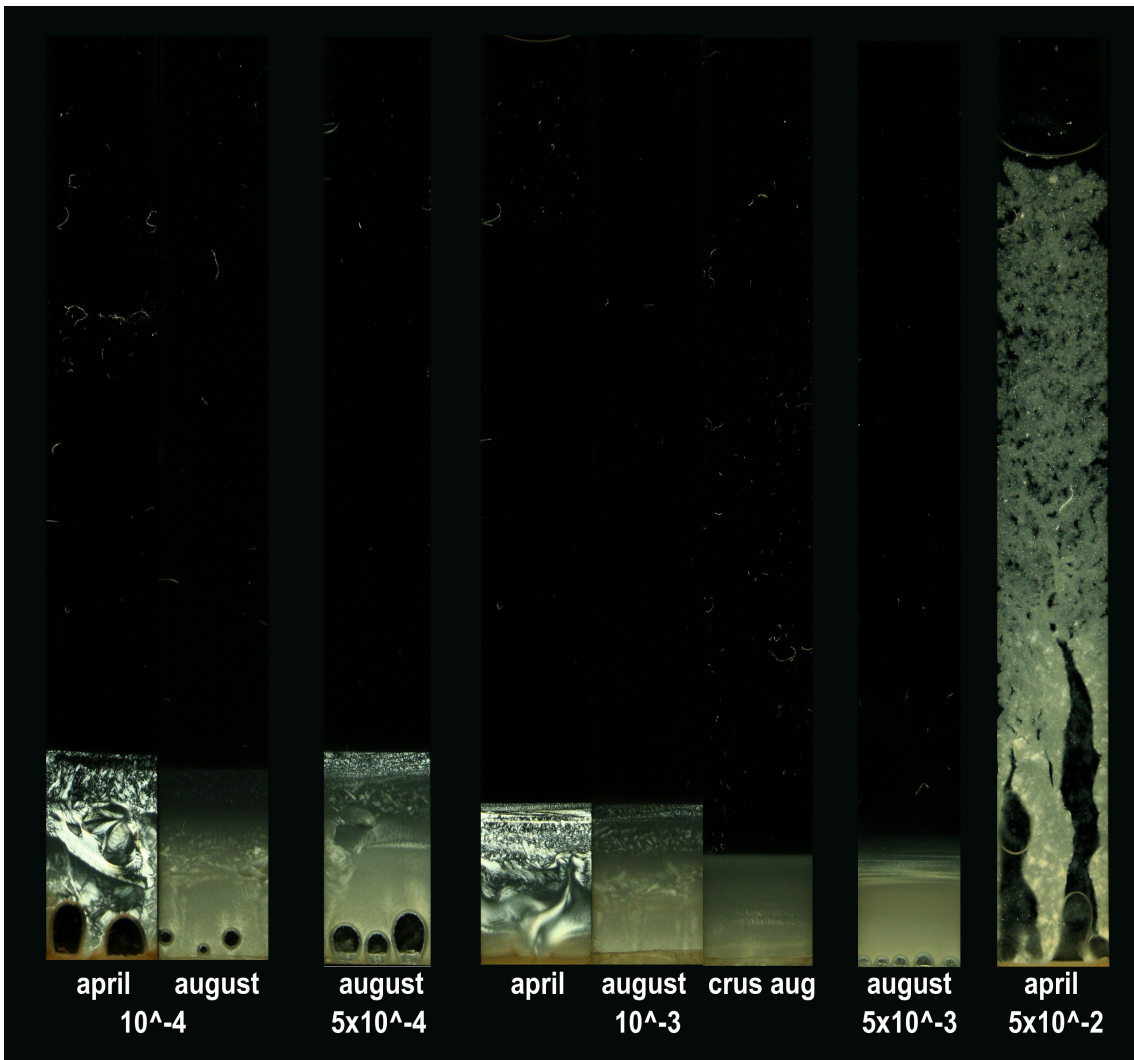


Figure 3.4: The 1 w/w% row showing comparisons of crushed April and uncrushed/crushed August. All of the three April samples are 5 months old, which is the oldest of all samples in the stock. The 1 % April samples differ from all other samples by being closed in the ends by silicon rubber. This can be seen by the orange color at the bottom end. Since the silicon has not sealed the tube very well, some large air bubbles can be seen at the lowest part. August  $10^{-4}$  M is only 11 days from the initial state and can not be fairly compared to the April sample. The August  $5 \times 10^{-4}$  M sample is 2 months old.

Since the cardboard setup was used for the 1 % April solutions, there has not been enough quality images to justify any movies for those samples. The time evolutions of these samples are therefore a bit uncertain due to large time gaps. Anyway, the 5 months shots looks pretty much close to some shots taken 2 months earlier.

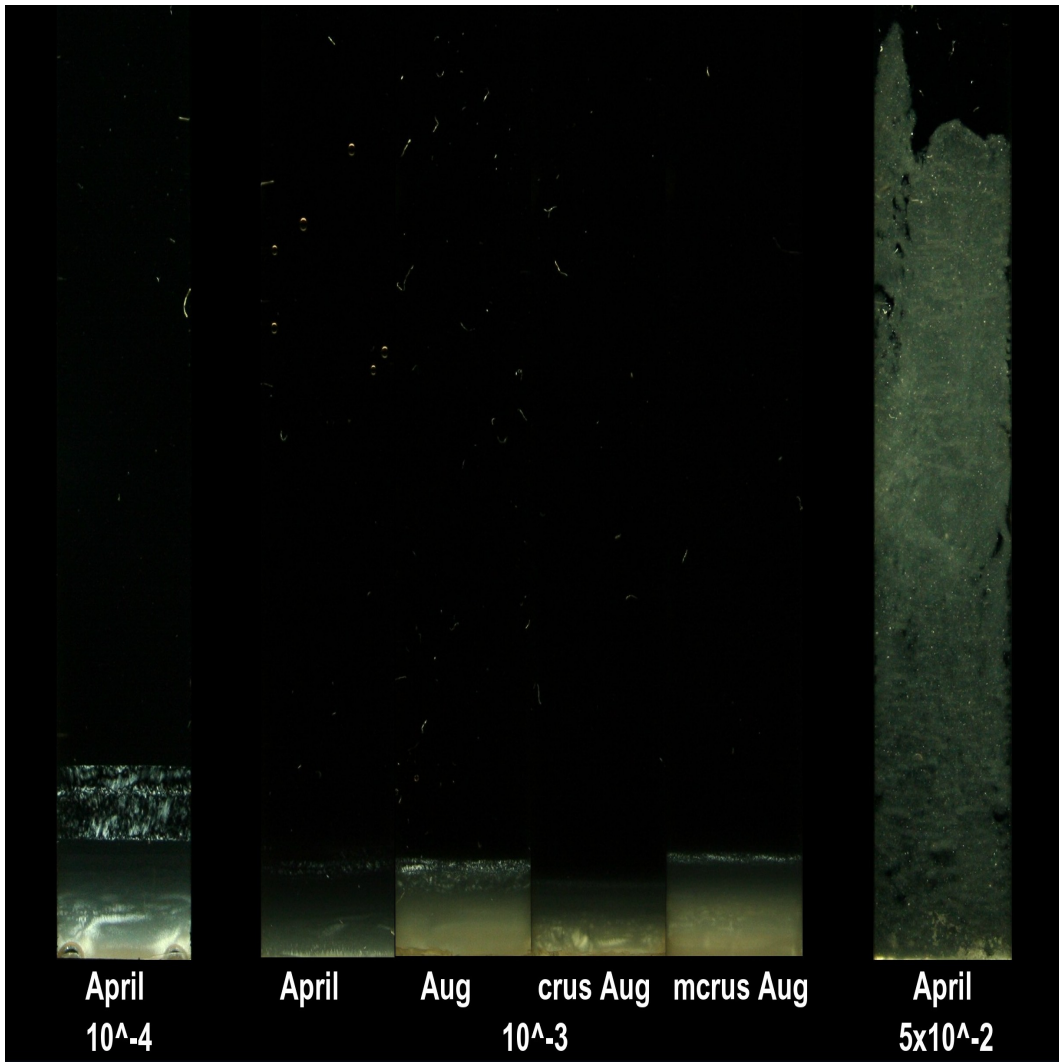


Figure 3.5: 0.5 w/w% row with four different sample types for  $10^{-3}$  M concentration. Both the  $10^{-4}$  M and  $5 \times 10^{-2}$  M samples are 75 days from initial state. All the pictures of the four types of  $10^{-3}$  M are shot 37 days after they were made. Except from the mortel crushed august (crus Aug) all the samples share the same hight. Uncrushed august (Aug) and the mechanical crushed august seem to have a similarity by having a clear birefringence at the upper phase. This make sense since the mechanical crushed sample just have been exposed to an extra treatment crushing of the same already crushed powder.

Figure 3.6 shows how much the powder preparation influences on the clays when dispersed in salt solution. The mortel crushed april powder, that will be closer examined in the next section, shows some very active dynamics in all directions. Because of the very fine crushing, the particle size from this powder can be assumed to be of a smaller size than the uncrushed sample next by. The uncrushed april sample shows some birefringence at the bottom upper above the smectic sedimentation. From the corresponding movie of this sample, all the clay movements in the sample can be seen to be attracted by the gravitational force. For the uncrushed august sample, until ten different phases can perhaps be distinkted, with a nematic phase identified as a variable texture change between some more smooth phases. The following mortel crushed august powder sample sure shows some interesting spots at the lower part, but the dynamics has been more or less absent compared to the equally crushed april powder. The mechanical crushed august

powder is unique in the way that it has a square frame birefringence pattern. It is hard to tell if this has arisen because of the tube edges, or it is caused by other reasons. The height from the bottom to the isotropic phase for the august samples are 5 cm and 3.5 cm for  $5 \times 10^{-4}$  M and  $10^{-3}$  M respectively. The  $5 \times 10^{-3}$  M sample does not after a 33 days time period have any distinct phase transitions, but by looking at the sedimentation rate and comparing to other samples, the height should probably end up between 2-3 cm. From table 1.1 the screening lenght for these three concentrations are 13 nm 10 nm and 4 nm for  $5 \times 10^{-4}$  M,  $10^{-3}$  M and  $5 \times 10^{-3}$  M concentrations. A 1.3 screening ratio for  $5 \times 10^{-4}$  M and  $10^{-3}$  M corresponds to an equal height ratio for these samples.

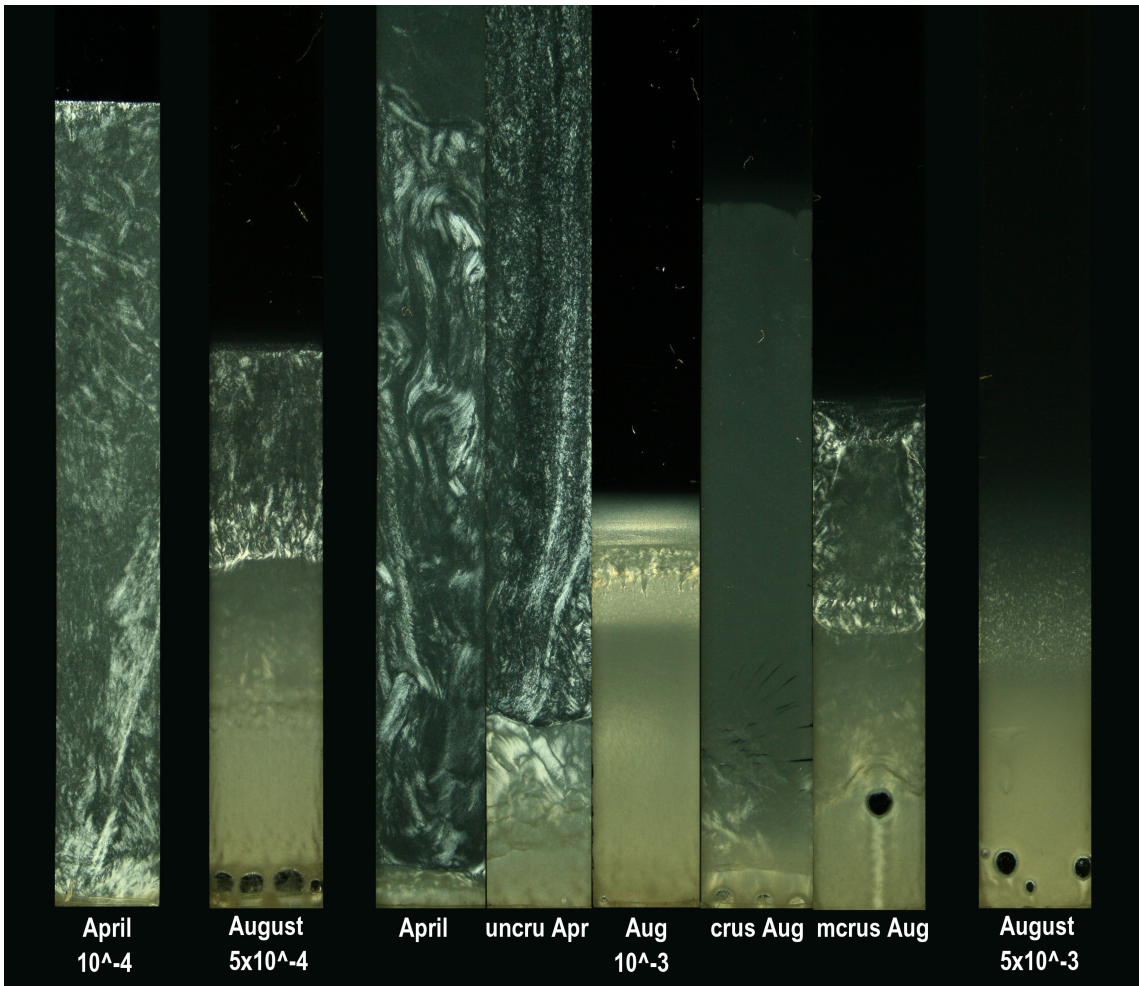


Figure 3.6: Row of 8 different samples 3 w/w%. Picture of april  $10^{-4}$  M is 70 days, august  $5 \times 10^{-4}$  M 15 days. April , uncrushed April, uncrushed august and crushed august for the  $10^{-3}$  M concentration are all 50 days old with the mechanical crushed sample being some 36 days.  $5 \times 10^{-3}$  M sample is 33 days from creation.

### 3.3 Comparison of w/w%

This section presents the different clay weight percentage for each concentration. Each figure contains some of the same pictures as above, but have in addition included some 4% samples. Figure 3.8, 3.9, 3.11 shows all the same tendency by having a more constant height increase when the clay weight percentage is increased. The  $5 \times 10^{-3}$  M concentra-

tion, summarized in figure 3.9, shows a clear shrink in nematic birefringence patterns. For the lowest concentrations it is more or less absent, at least as a higher layer. In the 1 month time period, the sample heights are not distributed proportionally to w/w%.

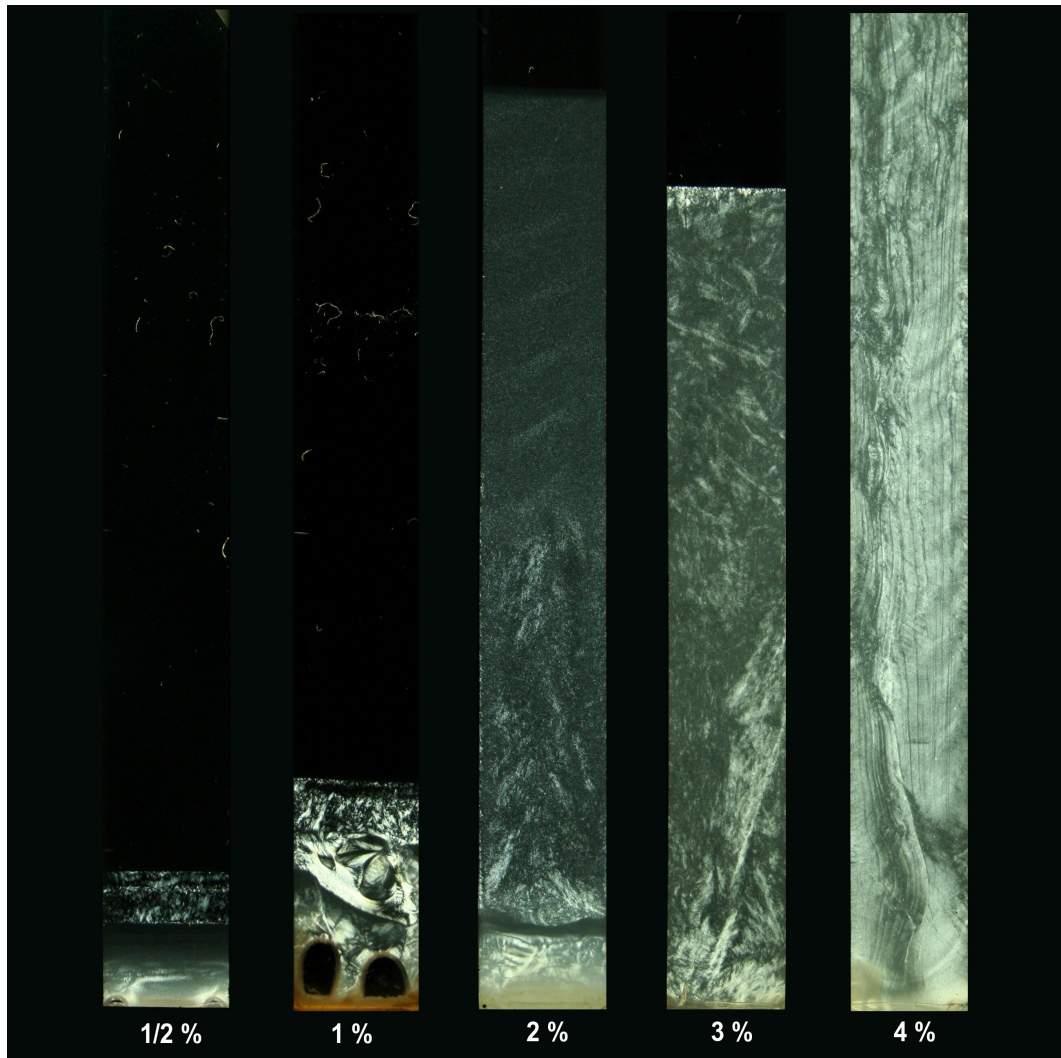


Figure 3.7: 5 samples of concentration  $10^{-4}$  with various April clay w/w%. The times from creations are 75 days, 5 months, 16 days, 70 days and 25 days for the 1/2%, 1%, 2%, 3% and 4% respectively. The 4 % sample is shot with an ISO value double as much as the others, giving it a bit brighter looks.

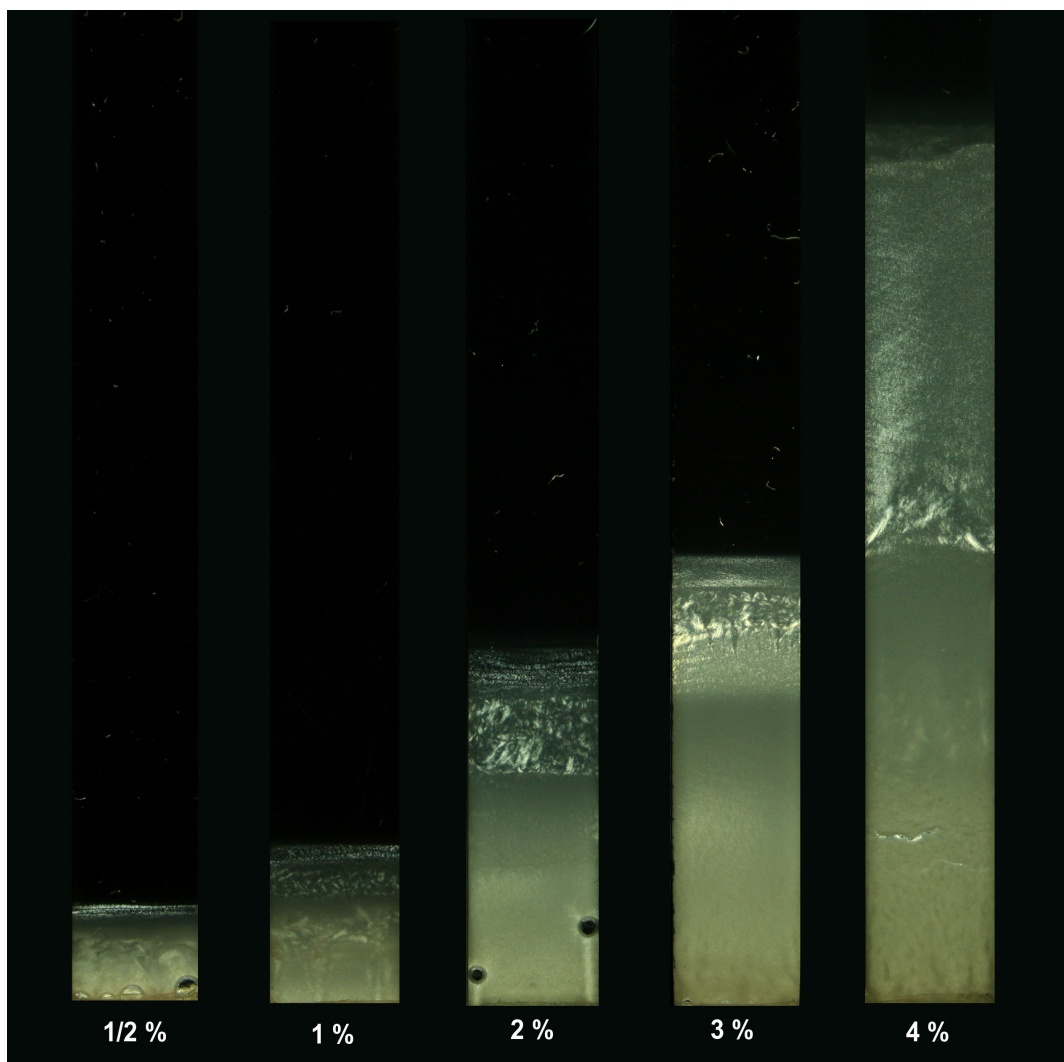


Figure 3.8: Five August samples of concentration  $10^{-3}$  with various clay w/w%. Times from creation vary from 37 - 47 days across the samples. Except from the 3% sample, which suffered from some vaporization, the height from bottom to isotropic are roughly in proportions to the corresponding increase in w/w%.

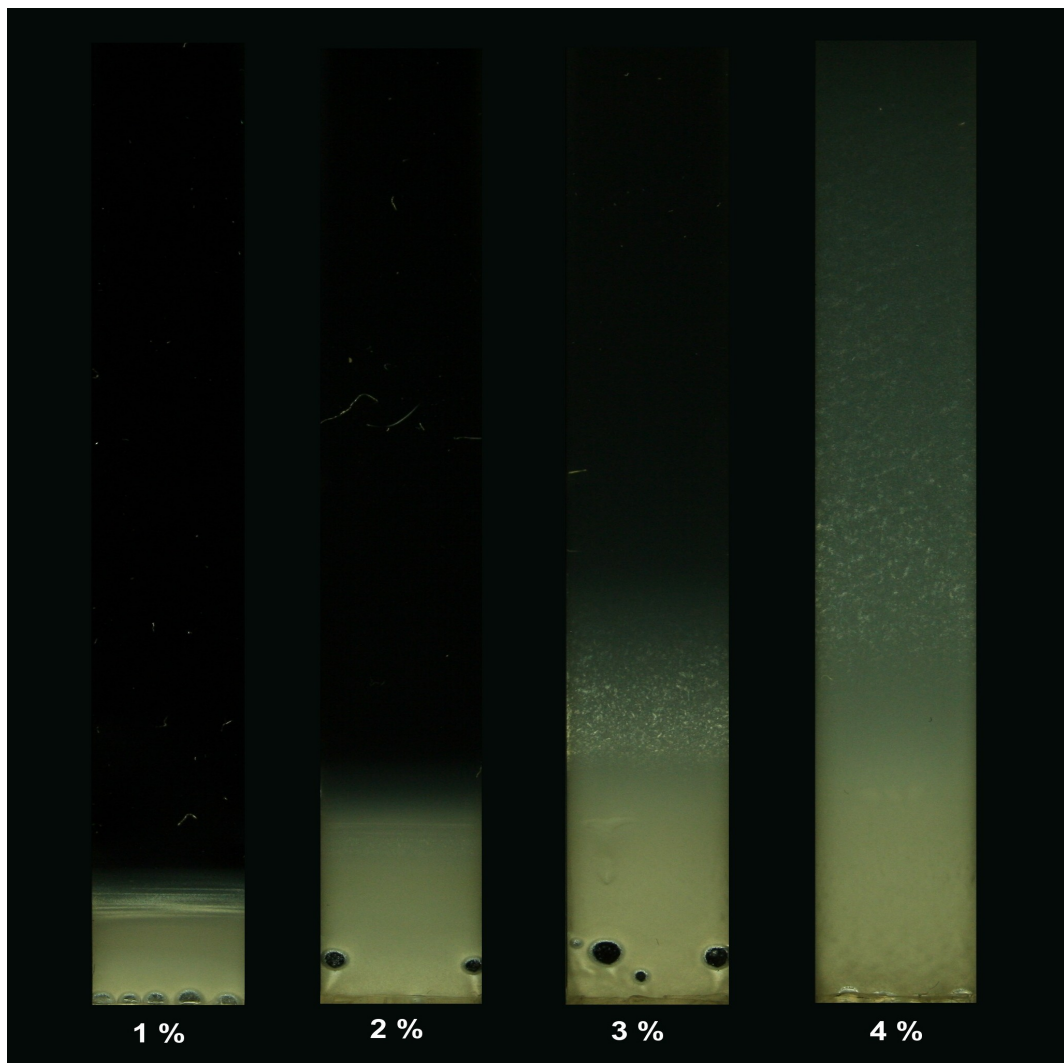


Figure 3.9: Four August samples of concentration  $5 \times 10^{-3}$  M. Times from creation are 2 months for the 1 % sample and 1 month for the rest. The 1 % sample looks nearly identical as it did one month earlier.

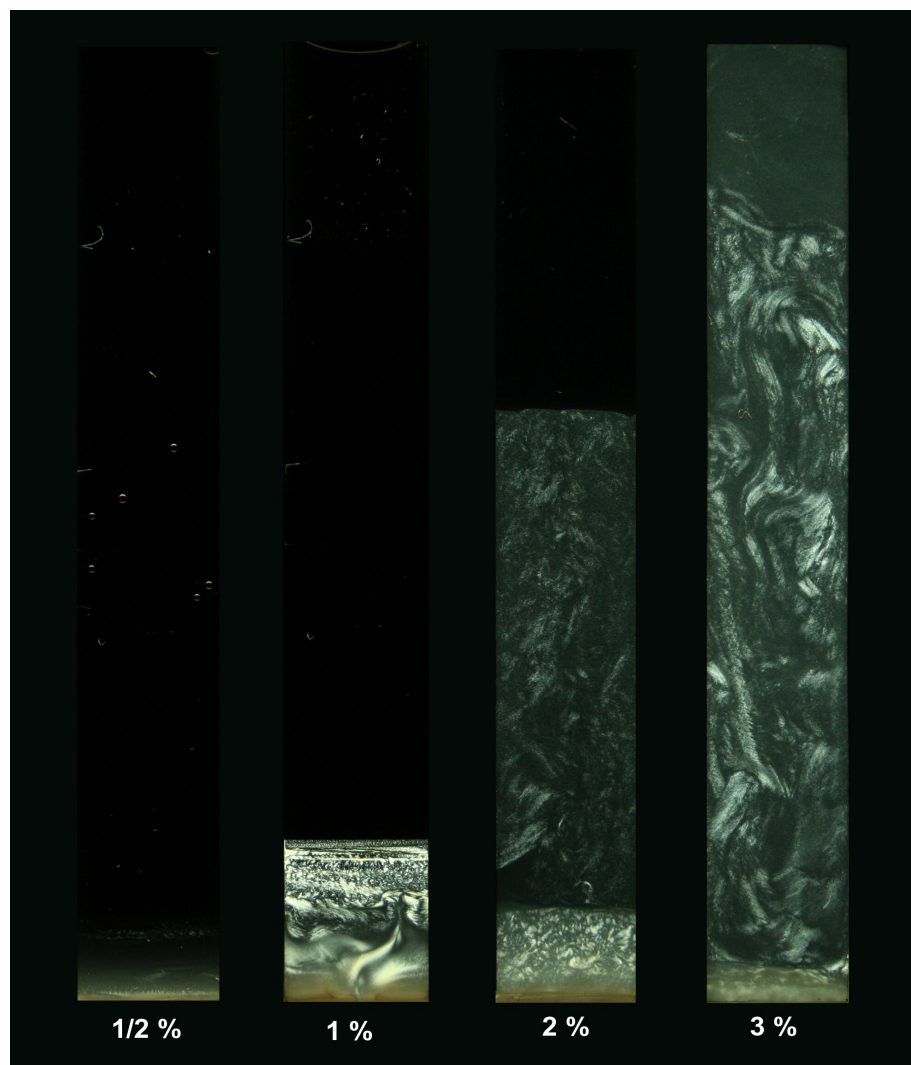


Figure 3.10: April  $10^{-3}$  M samples aligned with increasing w/w%. Times from creation are 37 days, 5 months, 37 days and 50 days for the 1/2 %, 1 %, 2 % and 3 % respectively.

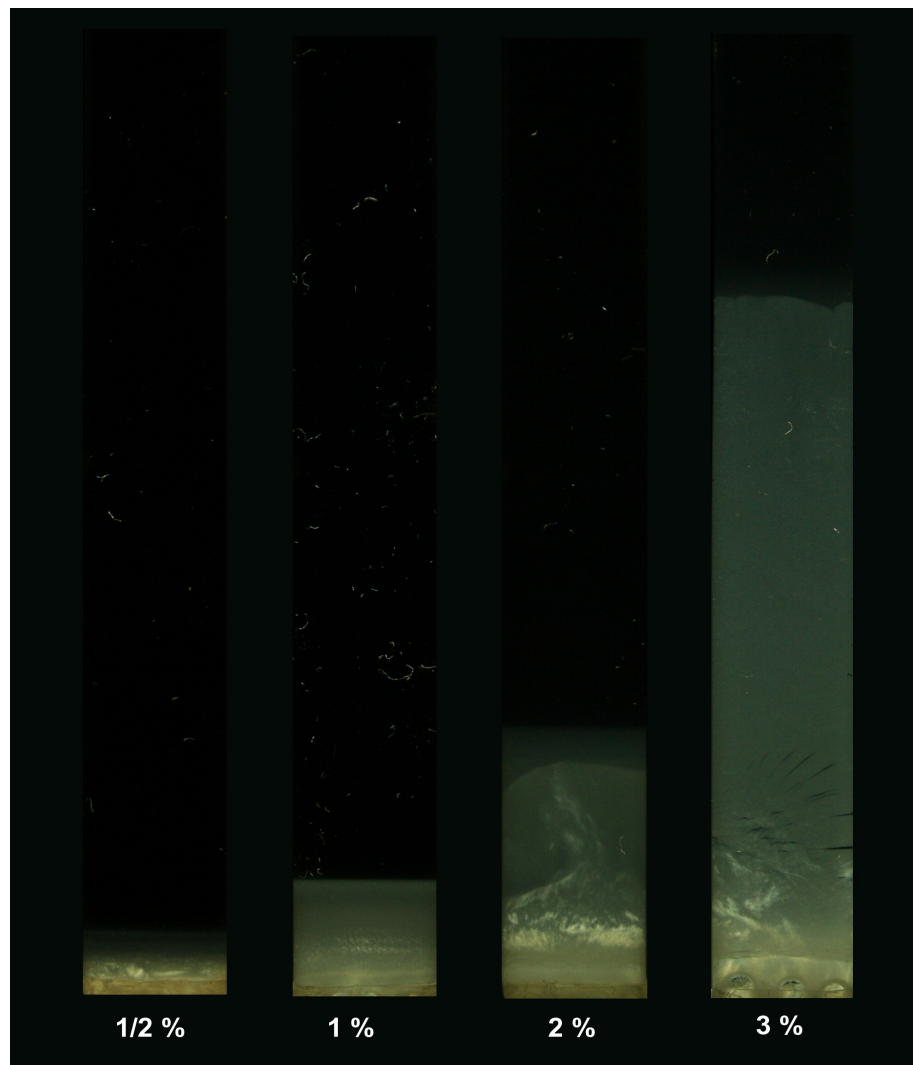


Figure 3.11: Mortel crushed August samples for  $10^{-3}$  Molar salt concentration. Time from creation is around 40 days for the samples.

### 3.4 Time progress

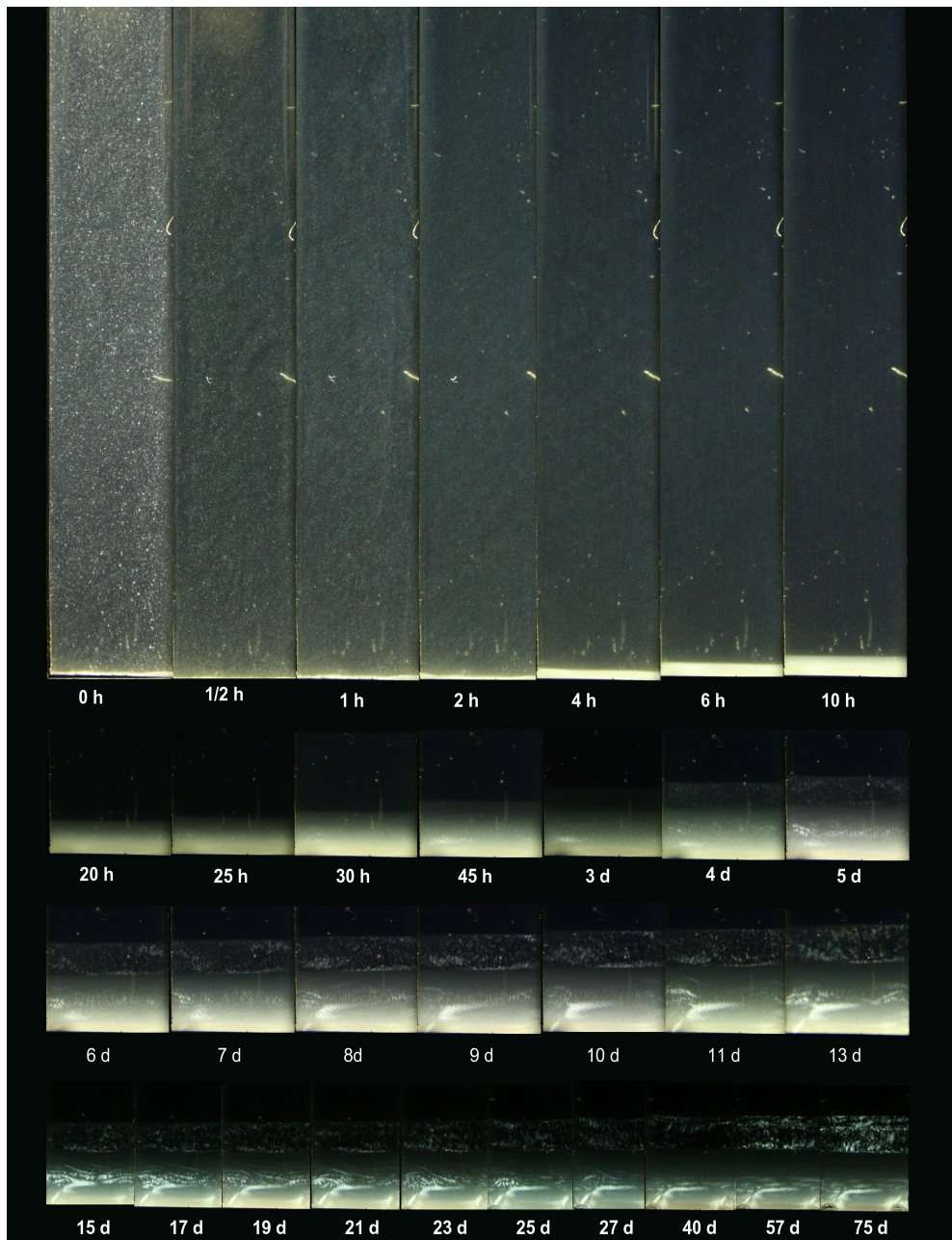


Figure 3.12: Time progress for  $10^{-4}$  Molar concentrated April solution. The light sensitivity of the shots in the first row have an ISO number of 1600. The rest of the pictures have ISO 800, which is used as standard for this sample. The use of this high ISO number might give a wrong impression for the lower phase since it appears much brighter than it should. The reason for the high light sensitivity is to better be able to spot the birefringence in upper phase. Even after 75 days this upper phase is constantly fluctuating

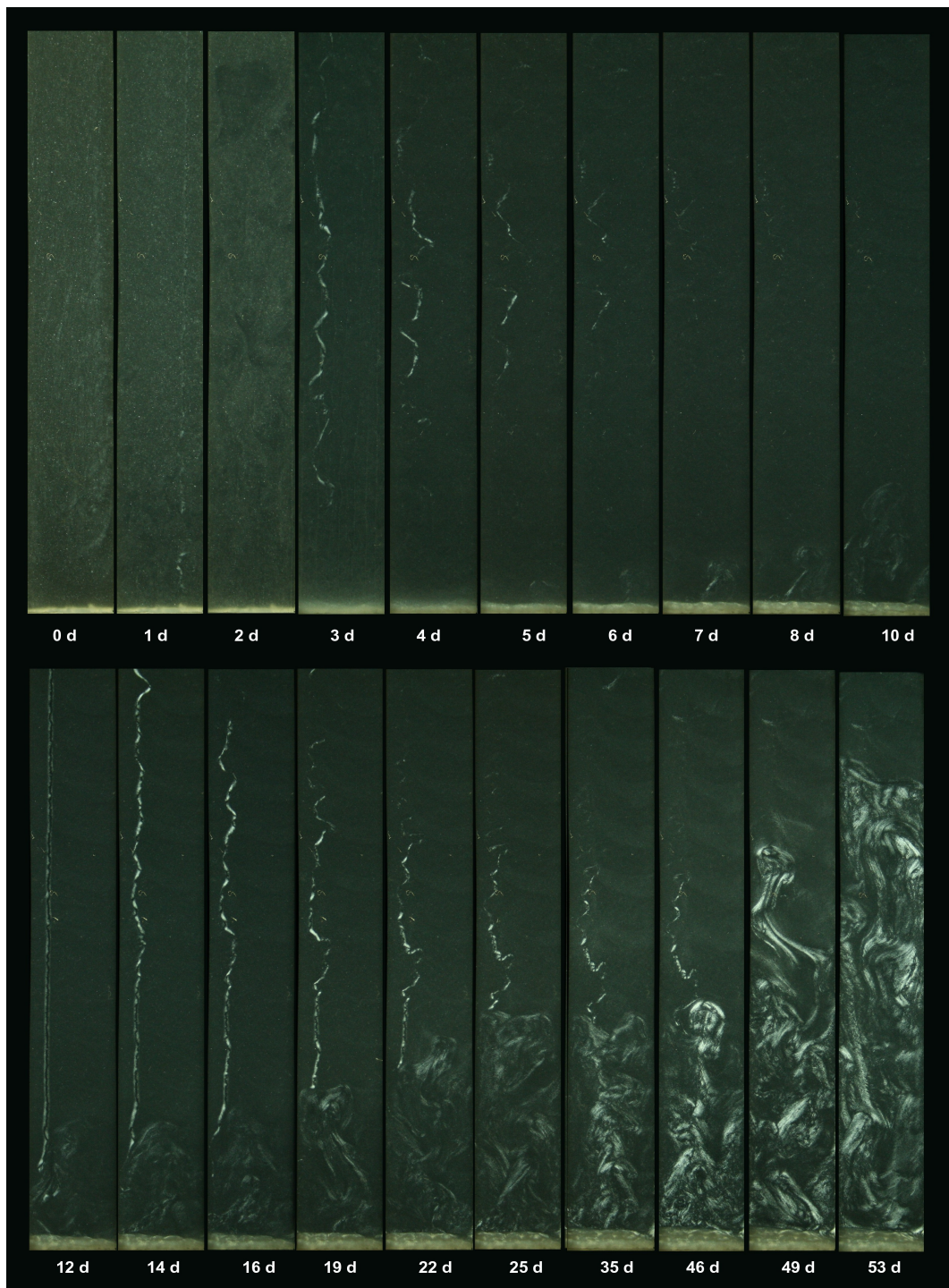


Figure 3.13: 53 days time progress for mortel crushed april in  $10^{-3}$  Molar salt solution. Of the interesting aspect for this sample, might be the coil that appear in the left part of the samples. This coil appears on the right side already in the beginning, but in a very hazy way. A new coil appear after 3 days for then disappear after 6-7 days. The strongest coil appears after some 12 days. This coil is in some way being slowly devoured by active dynamics.

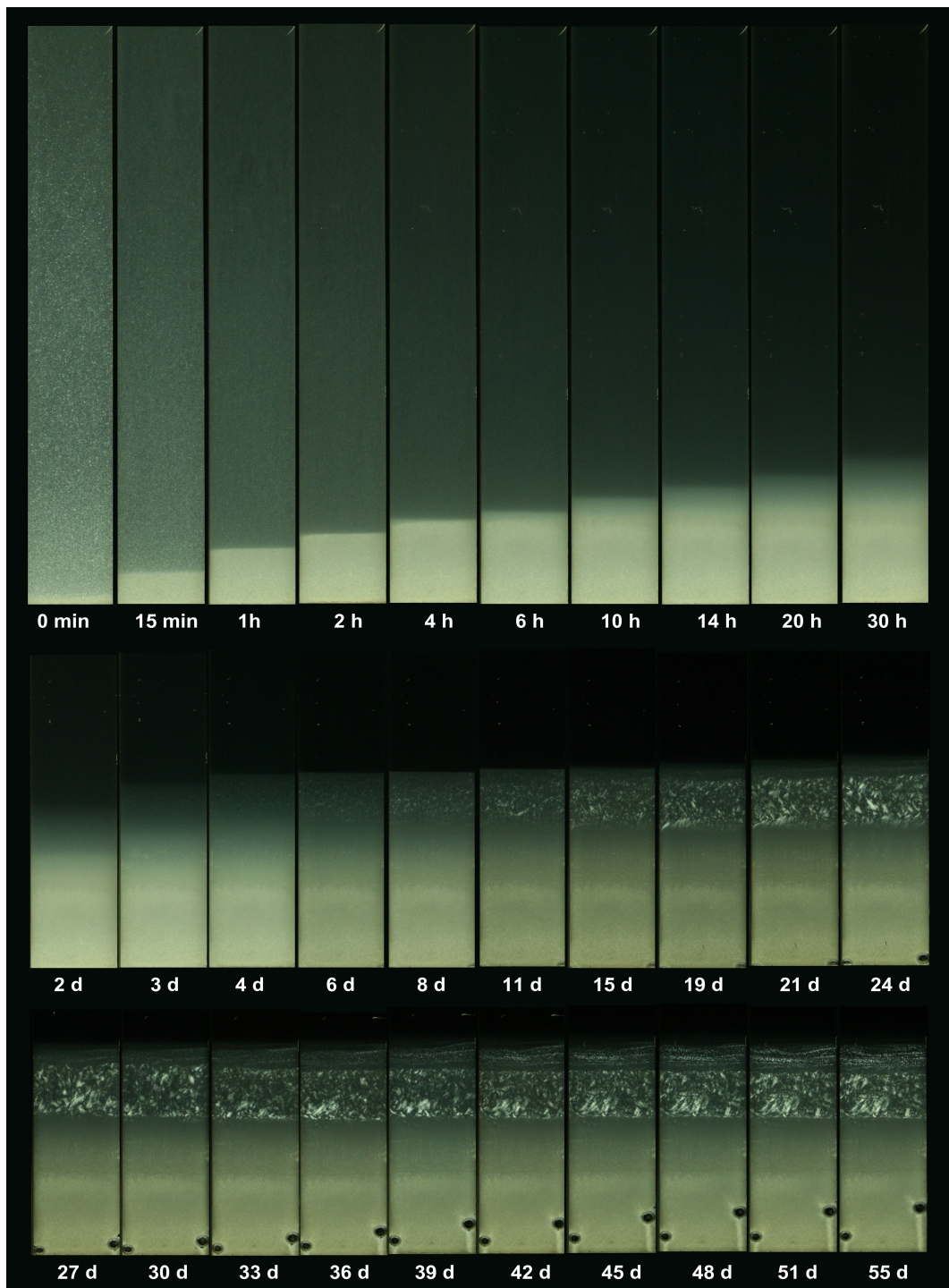


Figure 3.14: 55 days time progress of 2 % uncrushed august  $10^{-3}$  Molar salt concentraton. As can be seen from the first row, the uncrushed august powder has a very high sedimentation rate. As comparision, the crushed april powder and also the crushed august powder sediments much slower. The first phase after the heaviest sediment appears already after 6 hours. Some nematic phase birefringence starts to appear after 6-8 days. As can be better seen from this sample's movie, the dynamics in the nematic phase is very active in the first 40 days for then slowing down. A new birefringenced layer appear at the top after 45 days. This layer continues having constant dynamics.

### 3.5 Magnetic study

Figure 3.15 shows samples that have been settling under gravity with the influence of a magnetic field of strength 1 Tesla. Since the sampletubes have been standing with the flat side conducting the iron base of the magnet, the field lines has penetrated perpendicular on the samples as viewed in the paper. From the pictures the april sample seems to have undergone a change in birefringence, but the August sample remains unchanged. Since the april powder has smaller particles due to the mortel crushing, an indication could be that the magnetic field easier manage to influence particles with small sizes.

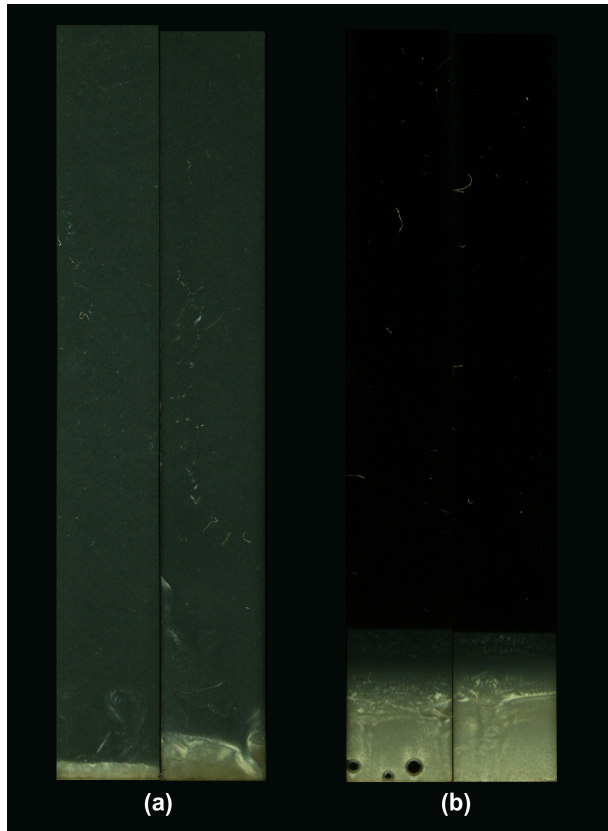


Figure 3.15: (a) Samples of 3 % april in a  $10^{-3}$  M concentration, both having an age of 13 days. The tube to the right is the magnetic sample, while the one to the left has settled under normal condition. As seen from the comparision the magnezied sample have a higher level of birefringence than the non-magnezied sample. Since none other reference sample has been made, it could be a bit unclear if this extra birefringence is due to magnetic influence. (b) 11 days samples of 1 % august solved in  $10^{-3}$  M solution. The sample to the right is the magnezied sample and the reference sample to the left. At first glans both samples looks more or less similar, thoug some closer inspection may suspect the magnetic sample to have some birefringence in the upper part. 11 days is anyway to little time to be able to get any good conlusions from this experiment.

### 3.6 Mass distribution of sample

Two samples of 3%  $10^{-3}$  M were made for april and august powder in a cutted 50 ml syringe. Figure 3.16 shows two equal reference samples in 50 ml glasses. For both samples there are a total of 180 measurepoints. The exact data can be found in a labjournal.

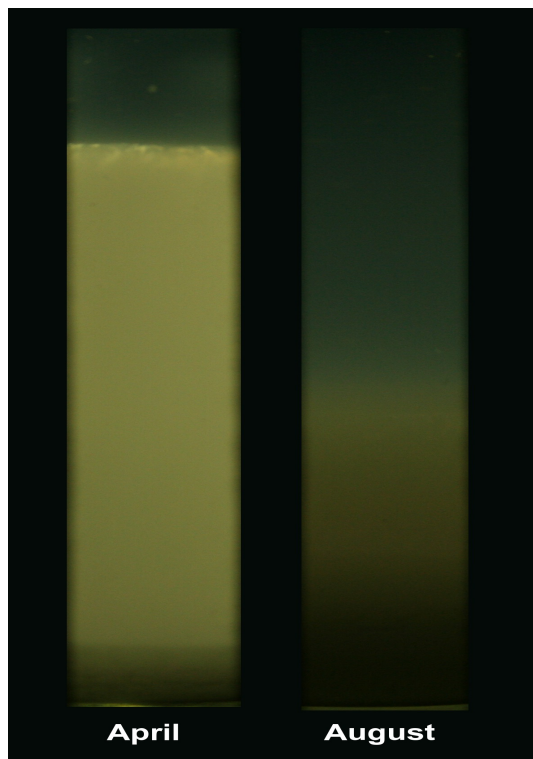


Figure 3.16: 3 % April and August samples of  $10^{-3}$  M concentration in 50 ml glasses placed between the crossed polarizers.

For both samples an equal amount of 250  $\mu\text{L}$  was taken out from the top of the syringes. Figure 3.17 and 3.18 shows the weight distribution for the two samples. Both the glasses and the syringes have the same dimensions; 7.5 cm high and diameter of 2.9 cm. Comparing figure 3.16 to the two graphs will explain their appearance. The weight in the isotropic phase is not constant through the phase, but tends to increase as it get closer to the phase transition.

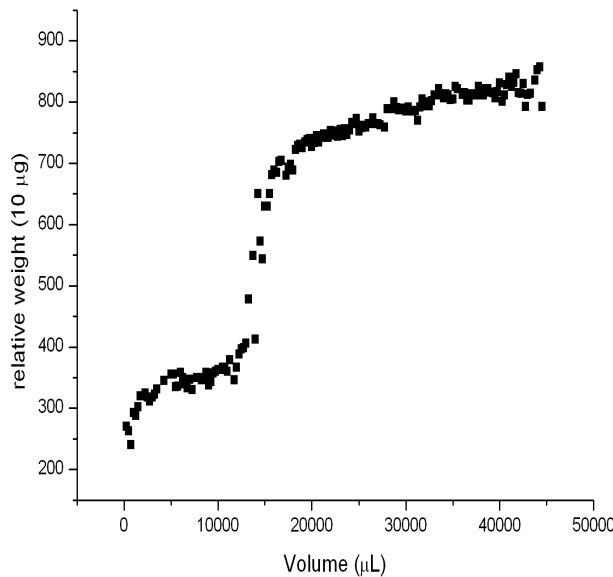


Figure 3.17: 3% April  $10^{-3}$  M. Volume corresponding to height as function of relative sample weight of  $250 \mu\text{m}$ . The leap at 15000 corresponds to the first distinct phase difference as seen in figure 3.16.

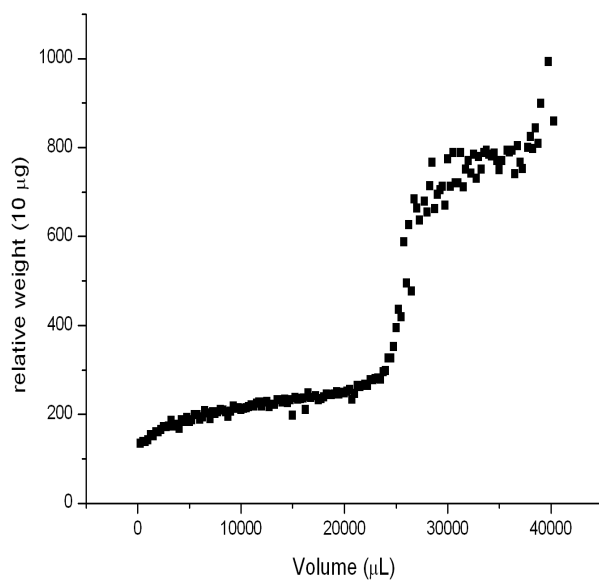


Figure 3.18: 3% August  $10^{-3}$  M. Volume corresponding to height as function of relative sample weight.

# Bibliography

- [1] (Brindley and Pedro, 1972)
- [2] P.D. Kaviratna, T.J. Pinnavaia and P.A. Schroeder. *J Phys Chem Solids* **57** (1996), p. 1897.
- [3] Introduction to clay minerals, B. Velde chapman Hall (1992)
- [4] J.-C.P. Gabriel, C. Sanchez and P. Davidson. *J Phys Chem* **100** (1996), p. 11139.
- [5] S.A.Solin, in *Chemical Physics of Intercalation II*, edited by P. Bernier *et al.* (Plenum Press, New York, 1993), p. 161.
- [6] Shah, M. J.; Thompson, D. C.; Hart, C. M. *J. Phys. Chem.* **1963**, 67, 1170.
- [7] Schweitzer, J.; Jennings, B. R. *J. Colloid Interface Sci.* **1971**, 37, 443.
- [8] Kasperski, K. L.; Hepler, C. T.; Hepler, L. G. *Can. J. Chem.* **1986**, 64, 1919.
- [9] Decruppe, J. P.; Hocquart, R.; Cressely, R. *Rheol. Acta* **1991**, 30, 575.
- [10] Thompson, D. W.; Butterworth, J. T. *J. Colloid Interface Sci.* **1991**, 151, 236.
- [11] Norris, J.; Giese, R. F.; Costanzo, P. M.; Van Oss, C. J. *Clay Miner.* **1993**, 28, 1.
- [12] Norrish, K. *Discuss. Faraday Soc.* **1954**, 18, 120.
- [13] Zou, J.; Pierre, A. C. *J. Mater. Sci. Lett.* **1992**, 11, 664.
- [14] Mourchid, A.; Delville, A.; Lambard, J.; Lecolier, E.; Levitz, P. *Langmuir* **1995**, 11, 1942.
- [15] Dijkstra, M.; Hansen, J. P.; Madden, P. A. *Phys. Rev. Lett.* **1995**, 75, 2236.
- [16] Langmuir, I. *J. Chem. Phys.* **1938**, 6, 873.
- [17] Emerson, W. W. *Nature* **1956**, 178, 1248.
- [18] Hight, R., Jr.; Higdon, W. T.; Schmidt, P. W. *J. Chem. Phys.* **1960**, 33, 1656.
- [19] Hight, R., Jr.; Higdon, W. T.; Darley, H. C. H.; Schmidt, P. W. *J. Chem. Phys.* **1962**, 37, 502.
- [20] Cebula, D. J.; Thomas, R. K.; White, J. W. *J. Chem. Soc., Faraday Trans. 1* **1980**, 76, 314.
- [21] Pons, C. H.; Rousseaux, F; Tchoubar, D. *Clay Miner.* **1981**, 17, 327.
- [22] Pons, C. H.; Rousseaux, F; Tchoubar, D. *Clay Miner.* **1982**, 16, 23.

- [23] Henderson, S. J.; White, J. W. *J. Appl. Crystallogr.* 1988, **21**, 744.
- [24] Avery, R. G.; Ramsay, J. D. F. *J. Colloid Interface Science* 1986, **109**, 448.
- [25] Ramsay, J. D. F.; Swanton, S. W.; Bunce, J. *J. Chem. Soc., Faraday Trans.* 1990, **86**, 3919.
- [26] Ramsay, J. D. F.; Lindner, P. *J. Chem. Soc., Faraday Trans.* 1993, **89**, 4207.
- [27] Braganza, L. F.; Crawford, R. J.; Smalley, M. V.; Thomas, R. K. *Clays Clay Miner.* 1990, **38**, 90.
- [28] Williams, G. D.; Moody, K. R.; Smalley, M. V.; King, S. M. *Clays Clay Miner.* 1994, **42**, 614.
- [29] Morvan, M.; Espinat, D.; Lambard, J.; Zemb, T. *Colloids Surf. A* 1994, **82**, 193.
- [30] Fripiat, J.; Cases, J.; Francois, M.; Letellier, M. *J. Colloid Interface Sci.* 1982, **89**, 378.
- [31] Fripiat, J.; Letellier, M.; Levitz, P. *Phil. Trans. R. Soc. London, A* 1984, **311**, 287.
- [32] Sur, S. K.; Heinsbergen, J. F.; Bryant, R. G. *J. Magn. Reson. A* 1993, **103**, 8.
- [33] J.-C.P. Gabriel, C. Sanchez and P. Davidson. *J Phys Chem* 100 (1996), p. 11139.
- [34] E. DiMasi, J.O. Fossum, T. Gog and C. Venkataraman. *Phys Rev E* **64**(2001), p. 61704.
- [35] B.J. Lemaire, P. Panine, J.-C.P. Gabriel and P. Davidson. *Europhys Lett* **59** (2002), p. 55.
- [36] J.D.F. Ramsay and P. Lindner. *J Chem Soc Faraday Trans* **89** (1993), p. 4207.
- [37] S.A. Solin. In: P. Bernier et al. *Chemical physics of intercalation II*, Plenum Press, New York (1993).
- [38] A. Mourchid, E. Lecolier, H. van Damme and P. Levitz. *Langmuir* 14 (1998), p. 4718.
- [39] M. Dijkstra, J.-P. Hansen and P.A. Madden. *Phys Rev E* **55** (1997), p. 3044.
- [40] R. Eppenga and D. Frenkel. *Mol Phys* **52** (1984), p. 1303
- [41] DE GENNES, P. G., 1974, *The Physics of Liquid Crystals* (Clarendon Press).
- [42] ONSACER, L., 1949, *Ann. N.Y. Acad. Sci.*, **51**, 627.
- [43] MAIER, W., and SAUPE, A., 1958, *Z. Naturf. A*, **13**, 564 ; 1959, *Ibid.*, **14**, 882 ; 1960, *Ibid.*, **15**, 287.
- [44] COTTER, M. A., 1979, *The Molecular Physics of Liquid Crystals*, edited by G. R. Luckhurst and G. W. Gray (Academic Press), p. 169.
- [45] BARBOY, B., and GELBART, W. M., 1980, *jT. statist. Phys.*, **22**, 709.
- [46] CHANDLER, D., WEEKS, J. D., and ANDERSEN, H. C., 1983, *Science, N.Y.*, **220**, 787.

- [47] LUCKHURST, G. R., 1979, *The Molecular Physics of Liquid Crystals*, edited by G. R. Luckhurst and G. W. Gray (Academic Press), p. 85.
- [48] SLUCKIN, T. J., and SHUKLA, P., 1983, *J. Phys. A*, **16**, 1539.
- [49] VIEILLARD-B and RoN, J., 1974, *Molec. Phys.*, **28**, 809.
- [50] REBERTUS, D. W., and SANDO, K. M., 1977, *J. chem. Phys.*, **67**, 2585. MONSON, P. A., and RtcnY, M., 1980, *Molec. Phys.*, **39**, 977. BOUBLIK, T., and NEZBEDA, I., 1980, *Czech. Phys. B*, **30**, 121.

## Appendix A

# Electromagnetic waves in an anisotropic material

Birefringence can be generally defined by considering a dielectric permittivity and a refractive index that are tensors. Consider a plane wave propagating in an anisotropic medium, with a relative permittivity tensor  $\epsilon$ , where the refractive index  $\mathbf{n}$ , is defined by  $\mathbf{n} \cdot \mathbf{n} = \epsilon$ . If the wave has an electric vector of the form:

$$\mathbf{E} = \mathbf{E}_0 i(\mathbf{k} \cdot \mathbf{r} - \omega t) \quad (\text{A.1})$$

where  $\mathbf{r}$  is the position vector and  $t$  is time, then the wave vector  $\mathbf{k}$  and the angular frequency  $\omega$  must satisfy Maxwell's equations in the medium, leading to the equations:

$$-\nabla \times \nabla \mathbf{E} = \frac{1}{c^2} \epsilon \frac{\delta^2 \mathbf{E}}{\delta t^2} \quad (\text{A.2})$$

$$\epsilon \mathbf{E} = 0 \quad (\text{A.3})$$

where  $c$  is the speed of light in a vacuum. Substituting equation (A.1) in equations (A.2) and (A.3) give the conditions:

$$|\mathbf{k}|^2 \mathbf{E}_0 - (\mathbf{k} \mathbf{E}_0) \mathbf{k} = \frac{\omega^2}{c^2} \epsilon \mathbf{E}_0 \quad (\text{A.4})$$

$$\mathbf{k} \epsilon \mathbf{E}_0 = 0 \quad (\text{A.5})$$

To find the allowed values of  $\mathbf{k}$ ,  $\mathbf{E}_0$  can be eliminated from equation A.4. One way to do this is to write equation (A.4) in Cartesian coordinates, where the x, y and z axes are chosen in the directions of the eigenvectors of  $\epsilon$ , so that

$$\epsilon = \begin{bmatrix} n_x^2 & 0 & 0 \\ 0 & n_y^2 & 0 \\ 0 & 0 & n_z^2 \end{bmatrix} \quad (\text{A.6})$$

Hence equation (A.4) becomes

$$(-k_y^2 - k_z^2 + \frac{\omega^2 n_x^2}{c^2} E_x + k_x k_y E_y + k_x k_z E_z = 0 \quad (\text{A.7})$$

$$k_x k_y E_x + (-k_x^2 - k_z^2 + \frac{\omega^2 n_y^2}{c^2} E_y + k_y k_z E_z = 0 \quad (\text{A.8})$$

$$k_x k_z E_x + (-k_x^2 - k_y^2 + \frac{\omega^2 n_z^2}{c^2} E_z + k_y k_z E_y = 0 \quad (\text{A.9})$$

where  $E_x$ ,  $E_y$ ,  $E_z$ ,  $k_x$ ,  $k_y$  and  $k_z$  are the components of  $\mathbf{E}_0$  and  $\mathbf{k}$ . This is a set of linear equations in  $E_x$ ,  $E_y$ ,  $E_z$ , and they have a solution if their determinant is zero:

$$\det \begin{bmatrix} (-k_y^2 - k_z^2 + \frac{\omega^2 n_x^2}{c^2}) & k_x k_y & k_x k_z \\ k_x k_y & (-k_x^2 - k_y^2 + \frac{\omega^2 n_z^2}{c^2}) & k_y k_z \\ k_x k_z & k_y k_z & (-k_x^2 - k_y^2 + \frac{\omega^2 n_x^2}{c^2}) \end{bmatrix} = 0 \quad (\text{A.10})$$

Multiplying out equation (A.10), and rearranging the terms, gives

$$\frac{\omega'}{c'} + \frac{\omega}{c^2} \left( \frac{k_x^2 + k_y^2}{n_z^2} + \frac{k_x^2 + k_z^2}{n_y^2} + \frac{k_y^2 + k_z^2}{n_x^2} \right) + \left( \frac{k_x^2}{n_y^2 n_z^2} + \frac{k_y^2}{n_x^2 n_z^2} + \frac{k_z^2}{n_x^2 n_y^2} \right) (k_x^2 + k_y^2 + k_z^2) = 0 \quad (\text{A.11})$$

In the case of a uniaxial material, where  $n_x = n_y = n_{\perp}$  and  $n_z = n_{\parallel}$  say, equation (A.11) can be factorised into

$$\left( \frac{k_x^2}{n_{\perp}^2} + \frac{k_y^2}{n_{\perp}^2} + \frac{k_z^2}{n_{\perp}^2} - \frac{\omega^2}{c^2} \right) \left( \frac{k_x^2}{n_{\parallel}^2} + \frac{k_y^2}{n_{\parallel}^2} + \frac{k_z^2}{n_{\perp}^2} - \frac{\omega^2}{c^2} \right) = 0 \quad (\text{A.12})$$

Each of the factors in equation (A.12) defines a surface in the space of vectors  $\mathbf{k}$  the surface of wave normals. The first factor defines a sphere and the second defines an ellipsoid. Therefore, for each direction of the wave normal, two wavevectors  $\mathbf{k}$  are allowed. Values of  $\mathbf{k}$  on the sphere correspond to the ordinary rays while values on the ellipsoid correspond to the extraordinary rays. For a biaxial material, eqn (A.11) cannot be factorised in the same way, and describes a more complicated pair of wave-normal surfaces. Birefringence is often measured for rays propagating along one of the optical axes (or measured in a two-dimensional material). In this case,  $\mathbf{n}$  has two eigenvalues which can be labelled  $n_1$  and  $n_2$ .  $\mathbf{n}$  can be diagonalised by:

$$\mathbf{n} = \mathcal{R}(\chi) \begin{bmatrix} n_1 & 0 \\ 0 & n_2 \end{bmatrix} \mathcal{R}(\chi)^T \quad (\text{A.13})$$

where  $\mathcal{R}(\chi)$  is the rotation matrix through an angle ( $\chi$ ). Rather than specifying the complete tensor  $\mathbf{n}$ , the magnitude of the birefringence may be specified by  $\Delta n$  and extinction angle ( $\chi$ ), where  $\Delta n = n_1 - n_2$ .

## Appendix B

### Drawings

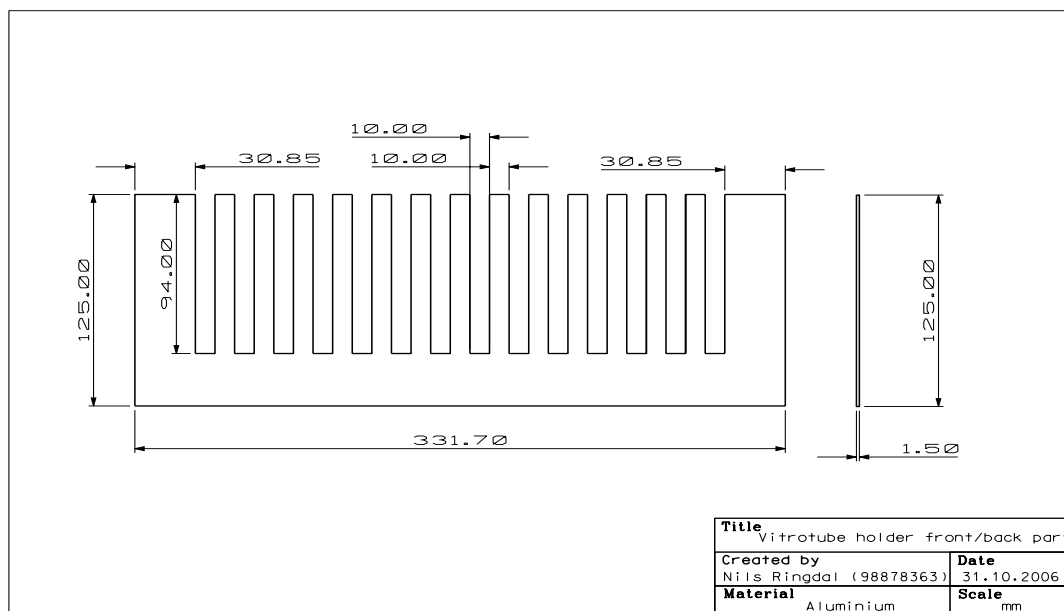


Figure B.1: The part that make up the two fronts of the sample rack.

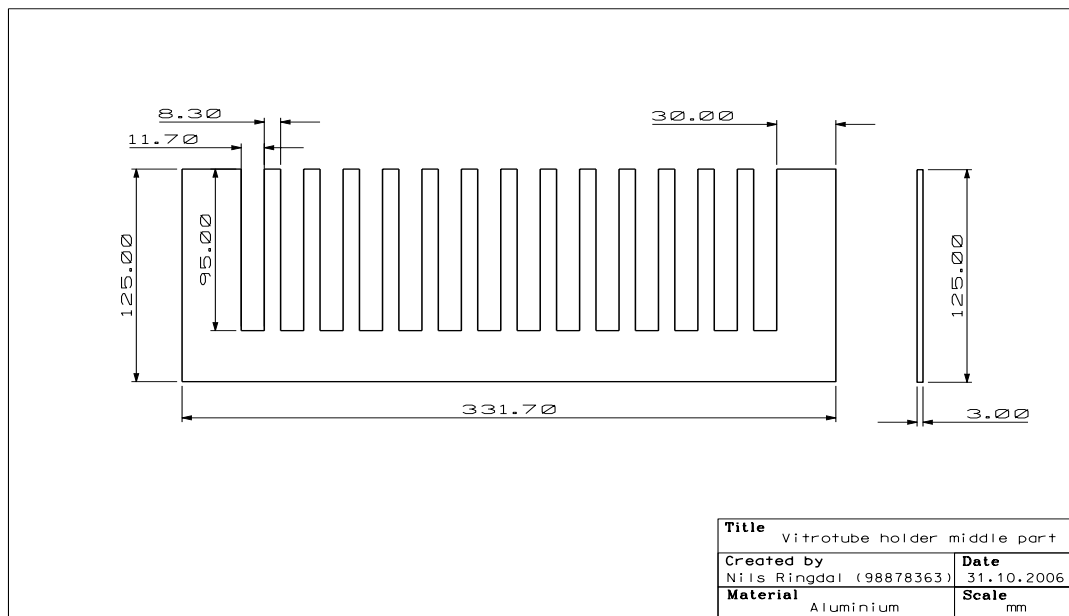


Figure B.2: The vitrotubes should fit in here.

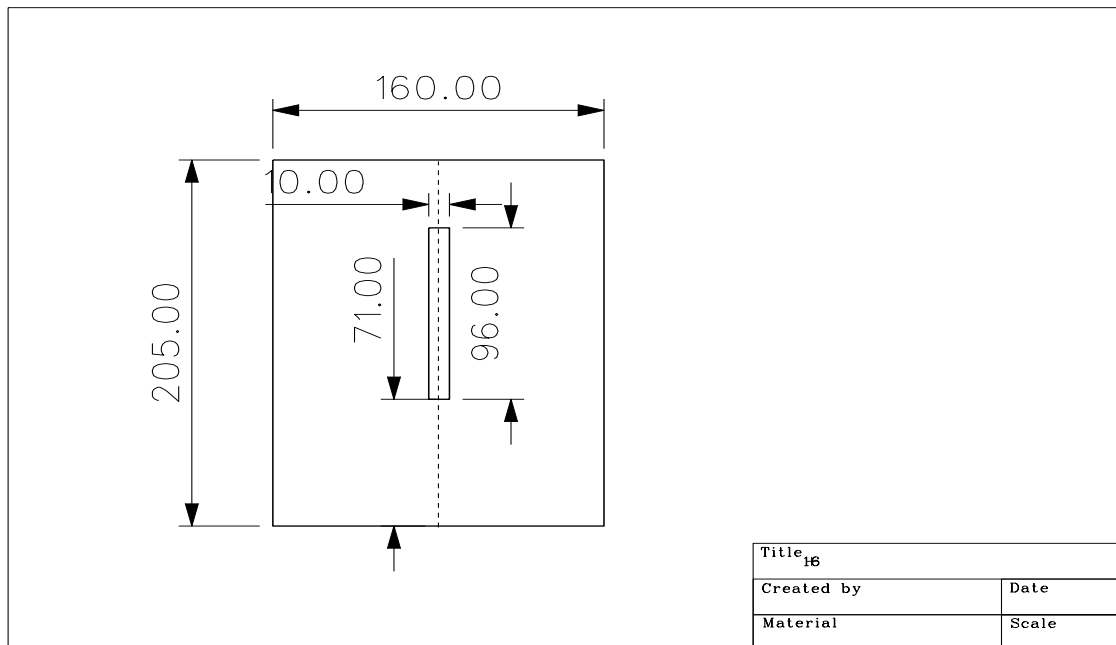


Figure B.3: This slit screen is between the camera and the samples.

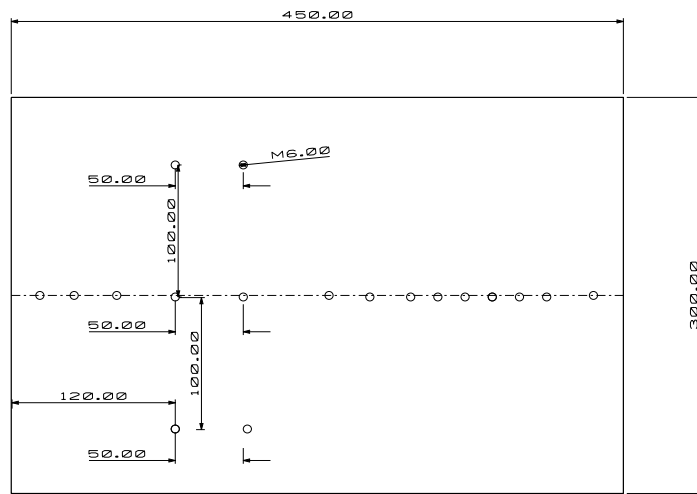


Figure B.4: This makes up the board for the camera, stage and polarizers.

## B.1 Rack

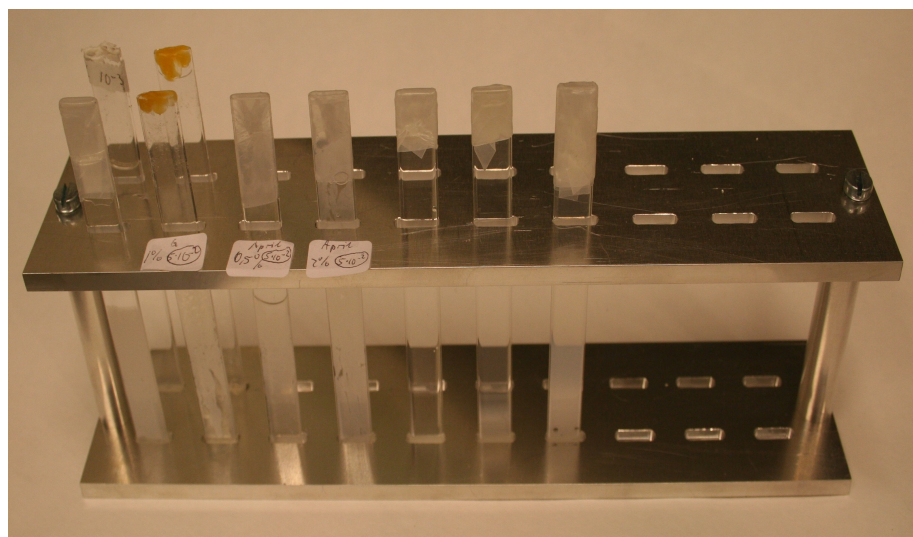


Figure B.5: A special designed rack for the vitrotubes. Drawings can be found on the DVD.